

1 The Arequipa massif of Peru: new SHRIMP and isotope constraints  
2 on a Paleoproterozoic inlier in the Grenvillian orogen.

3  
4  
5  
6  
7  
8  
9  
10  
11 C. Casquet<sup>a,\*</sup>, C.M. Fanning<sup>b</sup>, C. Galindo<sup>a</sup>, R.J. Pankhurst<sup>c</sup>, C. Rapela<sup>d</sup>, P.Torres<sup>e</sup>

12  
13  
14  
15  
16  
17  
18 <sup>a</sup> *Dpto. Petrología y Geoquímica, Fac.Ciencias Geológicas, Inst. Geología Económica. (CSIC,*  
19 *Universidad Complutense), 28040 Madrid, Spain*

20  
21  
22  
23  
24  
25  
26 <sup>b</sup> *Research School of Earth Sciences, The Australian National University, Canberra, ACT 200,*  
27 *Australia.*

28  
29  
30  
31  
32  
33  
34 <sup>c</sup> *British Geological Survey, Keyworth, Nottingham NG12 5GG, UK*

35  
36  
37  
38  
39  
40  
41 <sup>d</sup> *Centro de Investigaciones Geológicas, Universidad de La Plata, 1900, La Plata, Argentina.*

42  
43  
44  
45  
46  
47  
48 <sup>e</sup> *Universidad Nacional de Ingeniería, Av. Tupac Amaru 210, Lima, Perú*

49  
50  
51  
52  
53  
54  
55  
56  
57  
58  
59  
60  
61  
62  
63  
64  
65  
66  
67  
68  
69  
70  
71  
72  
73  
74  
75  
76  
77  
78  
79  
80  
81  
82  
83  
84  
85  
86  
87  
88  
89  
90  
91  
92  
93  
94  
95  
96  
97  
98  
99  
100  
101  
102  
103  
104  
105  
106  
107  
108  
109  
110  
111  
112  
113  
114  
115  
116  
117  
118  
119  
120  
121  
122  
123  
124  
125  
126  
127  
128  
129  
130  
131  
132  
133  
134  
135  
136  
137  
138  
139  
140  
141  
142  
143  
144  
145  
146  
147  
148  
149  
150  
151  
152  
153  
154  
155  
156  
157  
158  
159  
160  
161  
162  
163  
164  
165  
166  
167  
168  
169  
170  
171  
172  
173  
174  
175  
176  
177  
178  
179  
180  
181  
182  
183  
184  
185  
186  
187  
188  
189  
190  
191  
192  
193  
194  
195  
196  
197  
198  
199  
200  
201  
202  
203  
204  
205  
206  
207  
208  
209  
210  
211  
212  
213  
214  
215  
216  
217  
218  
219  
220  
221  
222  
223  
224  
225  
226  
227  
228  
229  
230  
231  
232  
233  
234  
235  
236  
237  
238  
239  
240  
241  
242  
243  
244  
245  
246  
247  
248  
249  
250  
251  
252  
253  
254  
255  
256  
257  
258  
259  
260  
261  
262  
263  
264  
265  
266  
267  
268  
269  
270  
271  
272  
273  
274  
275  
276  
277  
278  
279  
280  
281  
282  
283  
284  
285  
286  
287  
288  
289  
290  
291  
292  
293  
294  
295  
296  
297  
298  
299  
300  
301  
302  
303  
304  
305  
306  
307  
308  
309  
310  
311  
312  
313  
314  
315  
316  
317  
318  
319  
320  
321  
322  
323  
324  
325  
326  
327  
328  
329  
330  
331  
332  
333  
334  
335  
336  
337  
338  
339  
340  
341  
342  
343  
344  
345  
346  
347  
348  
349  
350  
351  
352  
353  
354  
355  
356  
357  
358  
359  
360  
361  
362  
363  
364  
365  
366  
367  
368  
369  
370  
371  
372  
373  
374  
375  
376  
377  
378  
379  
380  
381  
382  
383  
384  
385  
386  
387  
388  
389  
390  
391  
392  
393  
394  
395  
396  
397  
398  
399  
400  
401  
402  
403  
404  
405  
406  
407  
408  
409  
410  
411  
412  
413  
414  
415  
416  
417  
418  
419  
420  
421  
422  
423  
424  
425  
426  
427  
428  
429  
430  
431  
432  
433  
434  
435  
436  
437  
438  
439  
440  
441  
442  
443  
444  
445  
446  
447  
448  
449  
450  
451  
452  
453  
454  
455  
456  
457  
458  
459  
460  
461  
462  
463  
464  
465  
466  
467  
468  
469  
470  
471  
472  
473  
474  
475  
476  
477  
478  
479  
480  
481  
482  
483  
484  
485  
486  
487  
488  
489  
490  
491  
492  
493  
494  
495  
496  
497  
498  
499  
500  
501  
502  
503  
504  
505  
506  
507  
508  
509  
510  
511  
512  
513  
514  
515  
516  
517  
518  
519  
520  
521  
522  
523  
524  
525  
526  
527  
528  
529  
530  
531  
532  
533  
534  
535  
536  
537  
538  
539  
540  
541  
542  
543  
544  
545  
546  
547  
548  
549  
550  
551  
552  
553  
554  
555  
556  
557  
558  
559  
560  
561  
562  
563  
564  
565  
566  
567  
568  
569  
570  
571  
572  
573  
574  
575  
576  
577  
578  
579  
580  
581  
582  
583  
584  
585  
586  
587  
588  
589  
590  
591  
592  
593  
594  
595  
596  
597  
598  
599  
600  
601  
602  
603  
604  
605  
606  
607  
608  
609  
610  
611  
612  
613  
614  
615  
616  
617  
618  
619  
620  
621  
622  
623  
624  
625  
626  
627  
628  
629  
630  
631  
632  
633  
634  
635  
636  
637  
638  
639  
640  
641  
642  
643  
644  
645  
646  
647  
648  
649  
650  
651  
652  
653  
654  
655  
656  
657  
658  
659  
660  
661  
662  
663  
664  
665  
666  
667  
668  
669  
670  
671  
672  
673  
674  
675  
676  
677  
678  
679  
680  
681  
682  
683  
684  
685  
686  
687  
688  
689  
690  
691  
692  
693  
694  
695  
696  
697  
698  
699  
700  
701  
702  
703  
704  
705  
706  
707  
708  
709  
710  
711  
712  
713  
714  
715  
716  
717  
718  
719  
720  
721  
722  
723  
724  
725  
726  
727  
728  
729  
730  
731  
732  
733  
734  
735  
736  
737  
738  
739  
740  
741  
742  
743  
744  
745  
746  
747  
748  
749  
750  
751  
752  
753  
754  
755  
756  
757  
758  
759  
760  
761  
762  
763  
764  
765  
766  
767  
768  
769  
770  
771  
772  
773  
774  
775  
776  
777  
778  
779  
780  
781  
782  
783  
784  
785  
786  
787  
788  
789  
790  
791  
792  
793  
794  
795  
796  
797  
798  
799  
800  
801  
802  
803  
804  
805  
806  
807  
808  
809  
810  
811  
812  
813  
814  
815  
816  
817  
818  
819  
820  
821  
822  
823  
824  
825  
826  
827  
828  
829  
830  
831  
832  
833  
834  
835  
836  
837  
838  
839  
840  
841  
842  
843  
844  
845  
846  
847  
848  
849  
850  
851  
852  
853  
854  
855  
856  
857  
858  
859  
860  
861  
862  
863  
864  
865  
866  
867  
868  
869  
870  
871  
872  
873  
874  
875  
876  
877  
878  
879  
880  
881  
882  
883  
884  
885  
886  
887  
888  
889  
890  
891  
892  
893  
894  
895  
896  
897  
898  
899  
900  
901  
902  
903  
904  
905  
906  
907  
908  
909  
910  
911  
912  
913  
914  
915  
916  
917  
918  
919  
920  
921  
922  
923  
924  
925  
926  
927  
928  
929  
930  
931  
932  
933  
934  
935  
936  
937  
938  
939  
940  
941  
942  
943  
944  
945  
946  
947  
948  
949  
950  
951  
952  
953  
954  
955  
956  
957  
958  
959  
960  
961  
962  
963  
964  
965  
966  
967  
968  
969  
970  
971  
972  
973  
974  
975  
976  
977  
978  
979  
980  
981  
982  
983  
984  
985  
986  
987  
988  
989  
990  
991  
992  
993  
994  
995  
996  
997  
998  
999  
1000

- \*Corresponding author. Tel. +34 913944908; fax: +34 91
- E-mail address: [casquet@geo.ucm.es](mailto:casquet@geo.ucm.es)

18 **Abstract**

19  
20 The enigmatic Arequipa massif of southwestern Peru is an outcrop of Andean basement  
21 that underwent Grenvillian-age metamorphism. It is thus important to better constrain  
22 Laurentia–Amazonia ties in Rodinia reconstruction models. U-Pb SHRIMP zircon dating has  
23 yielded new evidence on the evolution of the massif between Middle Paleoproterozoic and  
24 Early Paleozoic. The oldest rock-forming events occurred in major orogenic events between  
25 *ca.* 1.79 and 2.1 Ga (Orosirian to Rhyacian), involving early magmatism (1.89–2.1Ga),

26 presumably through partly Archaean continental crust, sedimentation of a thick sequence of  
27 terrigenous sediments, UHT metamorphism at *ca.* 1.87 Ga, and late felsic magmatism at *ca.*  
28 1.79 Ga. The Atico sedimentary basin developed in the Late Mesoproterozoic and detrital  
29 zircons were fed from a source area similar to the high-grade Paleoproterozoic basement but  
30 also from an unknown source that provided Mesoproterozoic zircons of 1200–1600 Ma. The  
31 Grenville-age metamorphism was of low P-type and reworked the Paleoproterozoic rocks and  
32 also affected the Atico sedimentary rocks. Metamorphism was diachronous: *ca.* 1040 Ma in  
33 the Quilca and Camaná areas and in the San Juan Marcona domain,  $940 \pm 6$  Ma in the  
34 Mollendo area, and between 1000 and 850 Ma in the Atico domain. These metamorphic  
35 domains are probably tectonically juxtaposed. Comparison with coeval Grenvillian processes  
36 in Laurentia and in southern Amazonia opens the possibility that Grenvillian metamorphism  
37 in the Arequipa massif resulted from extension and not from collision. The Arequipa massif  
38 experienced Ordovician–Silurian magmatism at *ca.* 465 Ma, including anorthosites formerly  
39 considered to be Grenvillian, and high-T metamorphism within the magmatic arc. Focused  
40 retrogression along shear zones or unconformities took place between 430 and 440 Ma.

41 **Key words:** Arequipa, Grenvillian orogeny, Paleoproterozoic, U-Pb SHRIMP zircon dating,  
42 Rodinia.

## 45 **Introduction**

47 The Arequipa Massif (Cobbing and Pitcher, 1972) is an outcrop of metamorphic rocks and  
48 cross-cutting batholiths at least 800 km long and 100 km wide, along the desert coast of  
49 southern Peru (Shackleton et al., 1979), between the Andean Cordillera and the Chile–Peru  
50 trench (Fig. 1). It is part of the Andean basement that outcrops both as discontinuous inliers

1  
2  
3  
4  
5  
6  
7  
8  
9  
10  
11  
12  
13  
14  
15  
16  
17  
18  
19  
20  
21  
22  
23  
24  
25  
26  
27  
28  
29  
30  
31  
32  
33  
34  
35  
36  
37  
38  
39  
40  
41  
42  
43  
44  
45  
46  
47  
48  
49  
50  
51 throughout the belt and in uplifted blocks in the Andean foreland, from as far north as  
52 Venezuela to as far south as the Sierras Pampeanas of Argentina (see Rapela et al., this  
53 volume). Metamorphic rocks of the Arequipa Massif are mostly metasedimentary and range  
54 from amphibolite to granulite facies. Pervasive retrogression under greenschist facies was  
55 focused within late strongly sheared zones. Early dating of granulites between Camaná and  
56 Mollendo (Fig. 1) by Rb-Sr (whole-rock isochrons) and U-Pb (bulk dating of zircons) first  
57 resulted in Precambrian ages of ca 1.8–1.95 Ga (Cobbing et al., 1977; Dalmayrac et al., 1977;  
58 Shackleton et al., 1979). Regional metamorphism in the Arequipa Massif according to these  
59 authors resulted from a single Paleoproterozoic tectonothermal event; the age of sedimentary  
60 protoliths was estimated at *ca.* 2000 Ma. Emplacement of plutons and metamorphic  
61 reworking under low-grade conditions took place in the Paleozoic at *ca.* 450 Ma and *ca.* 390  
62 Ma (Shackleton et al., 1979).

63  
64 Paleogeographic models of Proterozoic continents as developed in the 1990s led to a  
65 renewed interest in the study of the Arequipa Massif. According to these models most  
66 continental masses reunited into a large supercontinent called Rodinia by the end of the  
67 Mesoproterozoic as a result of the Grenvillian orogeny (e.g. Moores, 1991; Hoffman, 1991;  
68 Dalziel, 1997). In these models, and in more recent paleogeographical reconstructions, the  
69 Amazonia craton figures juxtaposed to Laurentia, i.e., the ancestral North America craton, at  
70 *ca.* 1.0 Ga, although their relative positions vary from one to another (e.g., Dalziel, 1997;  
71 Davidson, 1995; Loewy et al., 2003; Tohver et al., 2004; Li et al., 2008). Amazonia broke  
72 away from Laurentia in the Neoproterozoic, leading to the opening of the Iapetus Ocean and  
73 the intervening Grenvillian orogen broke into conjugate belts along the margins of the rifted  
74 continents. Because Grenvillian ages were known from elsewhere in South America, lending  
75 credence to the Laurentia - Amazonia connection in this way, the age, paleogeography and

76 tectonics of the Arequipa Massif became the subject of thorough isotope (Nd and Pb) and  
77 renewed geochronological research (Wasteneys et al., 1995; Tosdal, 1996; Bock et al., 2000;  
78 Loewy et al., 2003, 2004).

80 U-Pb single-grain zircon dating of granulites yielded Grenvillian ages of *ca.* 1200 Ma near  
81 Quilca, and *ca.* 970 Ma near Mollendo for the high-grade metamorphism, with protolith ages  
82 of *ca.* 1.9 Ga (Wasteneys et al., 1995). The age of regional metamorphism in the Arequipa  
83 Massif thus switched from Paleoproterozoic to Late Mesoproterozoic and the massif was re-  
84 interpreted as having originated within the Grenville province. Further conventional zircon U-  
85 Pb dating was carried out by Loewy et al. (2004) on igneous gneisses of the San Juan and  
86 Mollendo areas. They inferred a complex history of crystallization of protoliths between 1851  
87 and 1818 Ma, and at *ca.* 1790 Ma, with development of an earlier gneissic fabric prior to the  
88 latter (M1 metamorphism). Mesoproterozoic metamorphism (M2) took place between *ca.*  
89 1052 Ma at San Juan and 935 Ma near Mollendo, suggesting a north-to-south younging of the  
90 metamorphic peak. A retrograde metamorphic overprint (M3) and conspicuous granite  
91 magmatism took place in the Ordovician at *ca.* 465 Ma (Loewy et al., 2003). Martignole and  
92 Martelat (2003) focused on the structure, geochronology and mineralogy of the high-grade  
93 metamorphism between Camaná and Mollendo, which they classified as of the UHT type  
94 ( $T > 900$  °C; 1.0–1.3 GPa) on account of ubiquitous peak assemblages with  
95 orthopyroxene+sillimanite+quartz and the local coexistence of sapphirine+quartz. Dating this  
96 metamorphism was attempted by *in situ* chemical (CHIME) U-Th-Pb determinations on  
97 monazites; the calculated ages range from 1064 to 956 ( $\pm 50$ ) Ma, with a peak *ca.* 1.0 Ga.

99 The Arequipa Massif has long been considered to be the northern exposure of a larger  
100 hypothetical continental block that outcrops as basement inliers within the Andean Cordillera

101 in northern Chile and northern Argentina, i.e., the composite Arequipa-Antofalla craton  
102 (Ramos, 1988). This block includes a Grenvillian basement and post-Grenvillian  
103 metamorphic and igneous overprints as young as 0.4 Ga (Loewy et al., 2003). Isotope (Nd  
104 and Pb) and geochronological considerations led Casquet et al. (2008) to establish  
105 comparisons between Grenvillian terranes recognized in the Western Sierras Pampeanas, i.e.,  
106 the Andean foreland, and the Arequipa Massif, thus enlarging the boundaries of the Arequipa-  
107 Antofalla block. However, both the role of the Arequipa Massif in the Grenvillian orogeny  
108 and its pre-Grenvillian history are still poorly known. Wasteneys et al. (1995) were the first to  
109 propose that the Arequipa Massif was a promontory of Laurentia accreted to Amazonía  
110 during the Sunsás orogeny, a Late Mesoproterozoic Grenvillian-age tectonic event long  
111 recognized along the SW margin of Amazonía, in Brasil and SE Bolivia (Litherland et al.,  
112 1989; Cordani and Teixeira, 2007). According to Wasteneys et al. (1995) granulite  
113 metamorphism resulted from pre-collisional subcontinental mantle delamination coeval with  
114 flat subduction, and concomitant rise of the hot asthenosphere that heated the overlying  
115 continental crust (see also Martignole and Martelat, 2003). However, for Loewy et al. (2004)  
116 the Arequipa-Antofalla block was an orphaned block, accreted to Amazonia during the  
117 Sunsás orogeny at *ca.* 1.05 Ga.

118  
119 It is now widely accepted that the Grenvillian orogenic cycle played an important role in  
120 Central Andean South America as evidenced by the Arequipa Massif and the Western Sierras  
121 Pampeanas. Moreover Grenvillian-age rocks have long been recognized in the basement of  
122 the Northern Andes (e.g., Restrepo Pace et al., 1997) and along the southern margin of the  
123 Amazonia craton (Cordani and Teixeira, 2007). However the pre-Grenvillian history and the  
124 time and mode of accretion of the Grenvillian terranes to nearby Amazonia, and correlations  
125 with the alleged Laurentian conjugate margin, still remain speculative.

126

1  
2 127 This contribution is aimed at better constraining the igneous and metamorphic history of  
3  
4 128 the Arequipa Massif by means of new U-Pb SHRIMP determinations and complementary  
5  
6  
7 129 geochemical evidence. We conclude that the massif was the site of a complex history that  
8  
9  
10 130 consisted of sedimentation, magmatism and metamorphism (UHT) in the Paleoproterozoic,  
11  
12 131 development of a sedimentary basin in the Mesoproterozoic, Grenville-age medium- to high-  
13  
14 132 grade metamorphism, and local metamorphic reworking and magmatism in the Early  
15  
16  
17 133 Paleozoic.

18  
19 134

20  
21  
22 135 **Geological setting**

23  
24 136

25  
26 137 The most comprehensive geological description of the Arequipa Massif is that of  
27  
28  
29 138 Shackleton et al. (1979). We retain here some of the domains that they distinguished to better  
30  
31 139 locate our samples. A summarized description follows based on their work and our own  
32  
33  
34 140 observations.

35  
36 141

37  
38  
39 142 The northern section

40  
41 143

42  
43 144 The *San Juan Marcona area* in the north (Fig. 1) consists of a basement and a discordant  
44  
45  
46 145 cover sequence. The latter is formed by glacial diamictites of the Chiquerio Formation  
47  
48  
49 146 followed by a carbonate cap, the San Juan Formation, both probably Neoproterozoic (Chew et  
50  
51 147 al., 2007). The basement consists of banded migmatitic gneisses and minor fine-grained  
52  
53 148 gneisses, strongly dismembered concordant pegmatites, concordant and discordant  
54  
55  
56 149 amphibolite dykes, and a foliated megacrystic granite of *ca.* 1790 Ma (Loewy et al., 2003).  
57  
58 150 Late granitic plutons cutting the discordance are Ordovician (Loewy et al., 2003). The *Atico*

59  
60  
61  
62  
63  
64  
65

151 *domain*, between Atico and Ocoña is medium-grade, with staurolite (+andalusite; Shackleton  
152 et al., 1979) schists, grey metasandstones, variably retrogressed amphibolites and concordant  
153 pegmatite sheets. Southward, this domain merges into a low-grade zone, *the Ocoña phyllonite*  
154 *zone*, that consists of strongly strained greenish chlorite-muscovite schists, grey  
155 metasandstones, quartz veins and concordant foliated pegmatite bodies. Shear bands, i.e., S-  
156 C' structures, are widespread and suggest that this is a shear zone with a top-to-the-NE sense  
157 of movement. Relics of an older foliation with discordant pegmatite dykes are locally  
158 preserved in strain shadows, outside which pegmatites are transposed to parallelism with the  
159 shear foliation. This shear zone was attributed to Paleozoic tectonism, probably Devonian, on  
160 structural grounds only (Shackleton et al., 1979). However, one foliated granite within the  
161 zone yielded an Ordovician age of *ca.* 464 Ma that is argued by Loewy et al. (2003) as shortly  
162 prior to the low-grade metamorphism (M3). The large *Atico igneous complex* consists in large  
163 part of diorites variably retrogressed to chlorite - epidote - albite, and abundant pegmatite  
164 dykes. This complex, along with its southern prolongation in the Camaná Igneous Complex,  
165 was attributed an age of *ca.* 450 Ma by Shackleton et al. (1979) on the basis of a combined  
166 Rb-Sr whole-rock isochron.

#### 168 The southern section

170 The *Camaná–Mollendo domain* is the largest one and consists of high-grade rocks that  
171 underwent granulite facies UHT metamorphism, with a paragenesis containing  
172 orthopyroxene+sillimanite+quartz and sapphirine+quartz (Martignole and Martelat, 2003). It  
173 consists for the most part of monotonous banded migmatitic gneisses formed by variably  
174 restitic mesosomes and alternating leucosomes (Fig. 2a). Augen-gneisses are found locally,  
175 such as near Mollendo, that probably formed by stretching of banded migmatites within

176 strongly strained shear zones. Peneconcordant but unstrained muscovite pegmatite sheets are  
177 irregularly distributed throughout the domain, more abundant in the north and northwest  
178 between Quilca and Camaná. Foliation is very regular over long distances. However changes  
179 in dip and strike can be mapped on a regional scale due to large upright post-foliation folds.  
180 Small-scale (cm to m) syn-foliation folds are locally found.

## 181 182 The Ilo domain

183  
184 The southernmost *Ilo domain* is separated from the main massif by a cover of Mesozoic  
185 and Cenozoic sedimentary rocks. This domain is a medium- to low-grade shear zone with  
186 strongly retrogressed igneous protoliths. The main facies is reddish, variably foliated,  
187 porphyritic granite. Boudins of coarse anorthosite that resulted from stretching of older larger  
188 bodies are aligned within the foliated porphyritic granite. A third facies consists of narrow  
189 bands, parallel to foliation, of a dark fine-grained mylonitic rock that contains irregularly  
190 distributed feldspar porphyroclasts. Contacts are sharp or gradual. Some bands look like  
191 sheared porphyritic granites; others as appear to be derived from dykes that underwent local  
192 mingling with the host granite. Strain increases from anorthosite through the dark bands to the  
193 granite; mylonitic foliation is common (Fig. 2b). Martignole et al. (2005) considered the  
194 protoliths to be part of a Grenvillian AMCG suite.

## 195 196 197 **Sampling and petrographic description**

198  
199 Out of a larger sampling of the whole massif from San Juan down to Ilo, eight samples  
200 were chosen for U-Pb SHRIMP dating of zircons and eight for Nd isotope composition. Two



201 muscovite samples were collected from pegmatites. Sampling was aimed at deciphering the  
202 complex geological history of this basement and particularly to constrain the age of the  
203 Grenvillian tectonothermal event. Because of the tectonic implications and the expected  
204 influence of the alleged Grenvillian anorthosite magmatism in UHT metamorphism (e.g.,  
205 Arima and Gower, 1991, and references therein) one target was the anorthosite and allied  
206 rocks from Ilo. Determining the protoliths of many of the metamorphic rocks was difficult,  
207 particularly for the highly recrystallized rocks of the Camaná–Mollendo domain, and so five  
208 high-grade gneisses from this domain were also analysed for REE.

209  
210 Sample locations are shown in Fig. 1. Coordinates, description, abbreviated mineralogy  
211 and the analytical work carried out on each sample are shown in Table 1. More detailed  
212 petrographic descriptions of the rocks can be found in Supplementary Table 1, obtainable  
213 from the Journal of South American Earth Sciences supplementary data file #1.

214

215

## 216 **Analytical methods**

217

218 REEs were analysed at ACTLABS (Canada) by ICP-MS (Table 4). Samples for Sr and Nd  
219 isotope analysis were crushed and powdered to ~ 200 mesh. Powders were first decomposed  
220 in 4 ml HF and 2 ml HNO<sub>3</sub> in Teflon digestion bombs for 48 hours at 120 °C, and finally in  
221 6M HCl. Elemental Rb, Sr, Sm and Nd were determined by isotope dilution using spikes  
222 enriched in <sup>87</sup>Rb, <sup>84</sup>Sr, <sup>149</sup>Sm and <sup>150</sup>Nd. Ion exchange techniques were used to separate the  
223 elements for isotopic analysis. Rb, Sr and REE were separated using Bio-Rad AG50 x 12  
224 cation exchange resin. Sm and Nd were further separated from the REE group using Bio-  
225 beads coated with 10% HDEHP. All isotopic analyses were carried out on a VG Sector 54

226 multicollector mass spectrometer at the Geocronología y Geoquímica Isotópica Laboratory,  
227 Complutense University, Madrid, Spain. Nd and Sr isotope data are shown in Tables 2 and 3  
228 respectively.

229  
230 U-Pb analyses were performed on eight samples using SHRIMP RG at the Research School  
231 of Earth Sciences, The Australian National University, Canberra. Zircon fragments were  
232 mounted in epoxy together with chips of the Temora reference zircon, ground approximately  
233 half-way through and polished. Reflected and transmitted light photomicrographs, and  
234 cathodo-luminescence (CL) SEM images, were used to decipher the internal structures of the  
235 sectioned grains and to target specific areas within the zircons. Each analysis consisted of 6  
236 scans through the mass range. The data were reduced in a manner similar to that described by  
237 Williams (1998, and references therein), using the SQUID Excel macro of Ludwig (2001). U-  
238 Pb data are in Supplementary Table 2 obtainable from the Journal of South American Earth  
239 Sciences Data Files 2#. Results are shown in Figs 3-5 and described below.

240

241

#### 242 **Zircon SHRIMP U-Pb samples and results**

243

244 *MAR-8*. Fine-grained gneiss (meta-igneous) (Fig. 3a). Zircons are elongate (less than  
245 150µm in length) sub-rounded to euhedral in shape. CL images show that most grains consist  
246 of a core and a rim. Cores are elongate euhedral prisms, although with resorption features,  
247 with oscillatory zoning that reflects an igneous origin. Rims show low luminescence and are  
248 large enough to be analysed.

249

250 Eighteen points were analysed including rims and cores. Nine cores yielded  $^{207}\text{Pb}/^{206}\text{Pb}$   
251 ages between 1210 and 1813 Ma. If analyses with discordance > 10% are rejected (#12 &  
252 #17), the remaining spots plot near Concordia and yield a mean  $^{207}\text{Pb}/^{206}\text{Pb}$  age of  $1796\pm 13$   
253 Ma (MSWD = 1.5), which is interpreted as the crystallization age of the igneous protolith.  
254 The high Th/U values of cores (0.32–0.34), typical of igneous zircons, reinforce this  
255 interpretation. Rims are high-U (mostly over 1000 ppm) and with very low Th/U values  
256 (mostly <0.2) typical of a metamorphic origin. Rim analyses plot on a discordia with an upper  
257 intercept at  $1033\pm 23$  Ma and a lower intercept at  $469\pm 70$  Ma; taken as the ages of Grenvillian  
258 metamorphism and early Paleozoic overprint, respectively. The latter gave rise to more  
259 pronounced Pb-loss in the Grenvillian rims than in the relict cores.

260  
261 *OCO-26*. Meta-sandstone (Fig. 3b). The zircons from this sample are mostly equant, round  
262 to sub-round grains that range up to 200  $\mu\text{m}$  in diameter but with many less than 50–100 $\mu\text{m}$ .  
263 The grains are generally clear and colourless, with only some clouded grains, and some that  
264 may be frosted due to surface transport. The CL images reveal a complex internal structure  
265 (Fig. 3b). Many grains comprise a zoned igneous centre, overgrown by metamorphic zircon  
266 with homogeneous CL. Also common are grains with metamorphic central areas with lighter  
267 or darker CL outermost metamorphic zircon. Some grains have multiple stages of zircon  
268 growth, the outermost invariably being a bright CL metamorphic rim.

269  
270 Given the complex nature of the zircon population, 105 areas were analysed on 70 zircon  
271 grains. The analyses range up to 30% discordant, although many are within analytical  
272 uncertainty of both the Wetherill ( $^{204}\text{Pb}$ -corrected data) and Tera-Wasserburg concordias (data  
273 uncorrected for common Pb). The relative probability plot shows a major peak at 1000 Ma,  
274 with slightly younger subordinate groups of analyses at *ca.* 940 Ma and *ca.* 840 Ma, a

1  
2  
3  
4  
5  
6  
7  
8  
9  
10  
11  
12  
13  
14  
15  
16  
17  
18  
19  
20  
21  
22  
23  
24  
25  
26  
27  
28  
29  
30  
31  
32  
33  
34  
35  
36  
37  
38  
39  
40  
41  
42  
43  
44  
45  
46  
47  
48  
49  
50  
51  
52  
53  
54  
55  
56  
57  
58  
59  
60  
61  
62  
63  
64  
65

275 sequence of minor peaks through the Mesoproterozoic (*ca.* 1200, 1260, 1340, 1500), and a  
276 significant concentration in the interval 1650–2030 Ma, as well as a few older ages back to  
277 2770 Ma (Archaean). The older ages are comparable to those seen in other samples reported  
278 here. We interpret the major peak at *ca.* 1000 Ma as corresponding to peak metamorphism of  
279 Grenville-age in the Atico domain. All older ages are interpreted as reflecting detrital grains,  
280 mostly igneous, but also metamorphic mantles.

281  
282 The data giving the youngest ages tend to plot above the Concordia curve in the Tera-  
283 Wasserburg diagram (not shown), in part forming a Pb-loss discordia. These areas are  
284 considered to have lost radiogenic Pb and are not interpreted as reflecting Neoproterozoic  
285 metamorphic zircon. However, the presence of ages of 850–950 Ma in the analyses of the  
286 outer areas and rims to structured grains record mean that a case can be made for  
287 metamorphic zircon development later than 1000 Ma.

288  
289 On the basis of this interpretation, peak metamorphism occurred at *ca.* 1000 Ma and the  
290 sedimentary protolith may well have formed between this time and the next oldest minor peak  
291 at *ca.* 1200 Ma, i.e., Late Mesoproterozoic.

292  
293 *CAM 2.* Migmatitic gneiss (mesosome) (Fig 4a). The zircons from this sample are equant  
294 to elongate, round to subround in shape and less than 200  $\mu\text{m}$  in length. The CL images  
295 reveal a range of internal structures. Some areas are zoned igneous zircon, whilst other areas  
296 have an irregular wispy structure, and yet others areas are broad and homogeneous. These  
297 features indicate a range of zircon crystallization events from simple igneous crystallization,  
298 to recrystallized zones and then finally metamorphic zircon growth.

299

300 Twenty-four areas were analysed on 21 zircon grains covering the range of internal CL  
301 structures, and yielding a bimodal distribution. In general the zoned igneous zircon yields  
302 older Proterozoic dates, whereas the more homogeneous metamorphic areas yield Grenvillian  
303 dates. But this is not always the case: the outer more homogeneous areas on grains #16 and  
304 #18 both yield older Proterozoic dates, whilst the weakly zoned area analysed on grain #17 is  
305 Grenvillian in age. Centres and rims were analysed on grains #10, #15 and #21. Both areas  
306 on grain #10 yield concordant Grenville dates, though the irregularly zoned core (#10.2) is  
307 older than the homogeneous metamorphic rim (#10.1). The irregularly zoned core of grain  
308 #15 is *ca.* 1960 Ma whereas the homogeneous rim is *ca.* 1050 Ma. The zoned core of grain  
309 #21 is *ca.* 1890 Ma, with the homogeneous rim Grenvillian at *ca.* 1040 Ma.

311 Overall, the older group consists of igneous and perhaps metamorphic core zircon with a  
312 range of nearly concordant  $^{207}\text{Pb}/^{206}\text{Pb}$  ages of 1760–1950 Ma, but with a composite peak at  
313 *ca.* 1900 Ma. The Grenvillian metamorphic group is rather variable with, at the older end, one  
314 concordant age at 1125 Ma and one less so at *ca.* 1210 Ma, and at the younger end, two  
315  $^{206}\text{Pb}/^{238}\text{U}$  ages less than 1000 Ma that probably indicate either Pb-loss of Grenvillian areas or  
316 a superimposed thermal event peaking at *ca.* 980 Ma. The weighted average of the six  
317 remaining  $^{206}\text{Pb}/^{238}\text{Pb}$  ages is  $1040\pm 11$  (MSWD = 0.90), which is taken as the peak of  
318 Grenvillian metamorphism.

320 *CAM-7*. Migmatitic gneiss (mesosome) (Fig 4b). The zircons from this sample are round,  
321 equant-to-elongate grains that range from less than 100  $\mu\text{m}$  in diameter to 200  $\mu\text{m}$  or more in  
322 length. A few multi-lobate grains are present, representing metamorphic overgrowths. The CL  
323 images, as of sample CAM 2 show a variety of textures and features. There are areas of

324 zoned igneous zircon, usually more centrally located within the grains, with both irregular and  
325 homogenous CL structures in outer areas (mantles) and rims.

326  
327 Twenty-seven areas have been analysed on 20 zircon grains with rim-and-core pairs  
328 analysed for seven grains. The zoned igneous core to grain #17 has an Archaean  $^{207}\text{Pb}/^{206}\text{Pb}$   
329 age of  $\sim 2690$  Ma whereas the more homogeneous rim area, interpreted as metamorphic, is  
330 Grenvillian in age with a  $^{206}\text{Pb}/^{238}\text{U}$  date of  $\sim 1120$  Ma. The outer areas and zoned igneous  
331 zircons provide a range of nearly concordant  $^{207}\text{Pb}/^{206}\text{Pb}$  dates, mostly around 1860 to 2080  
332 Ma. The Wetherill plot for the  $^{204}\text{Pb}$ -corrected data clearly shows that whilst some areas are  
333 near Concordia at about either 1950 Ma or 1000 Ma, many of the areas analysed are  
334 discordant and would lie on a simple discordia between these two end-members. A discordia  
335 line fitted to a selected group of 22 analyses gives an upper intercept of  $1924 \pm 25$  Ma and  
336 lower intercept of  $1026 \pm 32$  Ma (MSWD = 3.7), the latter being taken as the age of peak  
337 Grenvillian metamorphism. The analyses not included in this general discordia line are for  
338 #15.2, with the youngest  $^{207}\text{Pb}/^{206}\text{Pb}$  date, and those with  $^{207}\text{Pb}/^{206}\text{Pb}$  dates older than 2000  
339 Ma.

340  
341 From the current data set it is clear that detrital igneous zircon and probably overgrowths  
342 of Paleoproterozoic age are common in this sample. New zircon formed during a Grenville-  
343 age event is present. A number of the grains/areas analysed show variable radiogenic Pb-loss  
344 at this time and so lie on a discordia trend.

345  
346 *QUI-16*. Migmatitic gneiss (mesosome) (Fig. 4c). Separated zircons are mostly *ca.* 200  $\mu\text{m}$   
347 in length, equant to slightly elongated, and sub-round in form. CL images show complex  
348 internal structures, with small relict cores (in some cases with igneous zoning) surrounded by

1  
2  
3  
4  
5  
6  
7  
8  
9  
10  
11  
12  
13  
14  
15  
16  
17  
18  
19  
20  
21  
22  
23  
24  
25  
26  
27  
28  
29  
30  
31  
32  
33  
34  
35  
36  
37  
38  
39  
40  
41  
42  
43  
44  
45  
46  
47  
48  
49  
50  
51  
52  
53  
54  
55  
56  
57  
58  
59  
60  
61  
62  
63  
64  
65

349 mantles of variable thickness most of which show broad faint oscillatory zoning, and low-  
350 luminescence rims. The latter are usually complete and discordant to the earlier structures;  
351 they are of irregular thickness, up to 50  $\mu\text{m}$  or more on some grain tips. The textures are  
352 interpreted as due to detrital igneous crystals and successive stages, probably two, of  
353 metamorphic overgrowth.

354  
355 Sixteen areas were analyzed on 15 grains. Both core and mantle were analysed in grain #1.  
356 Two analyses (# 4 and #8) were carried out on well-developed rims; their  $^{207}\text{Pb}/^{206}\text{Pb}$  ages are  
357 1079 Ma and 1995 Ma. The other spots were on mantles: Th/U ratios are generally high  
358 (0.07–3.33, with 12 out of 16 ratios being  $> 0.2$ ). If the more imprecise analyses are excluded,  
359 the rest plot on a simple Discordia (MSWD = 0.9) with an upper intercept at  $1861 \pm 32$  Ma and  
360 a poorly defined lower intercept at  $1011 \pm 73$  Ma.

361  
362 *MOL-17*. Augen-gneiss (uncertain protolith) (Fig. 4d). The zircons from this sample are  
363 round to subround grains that are generally clear. The CL images show complex internal  
364 structure; many grains have zoned igneous cores, interpreted as igneous, overgrown by more  
365 homogeneous, probably metamorphic zircon.

366  
367 Sixteen grains were analysed, with most of the analyses on the more homogeneous outer  
368 areas of the grains interpreted as metamorphic. The exceptions are the analyses of grain #16,  
369 where the zoned core was also analysed (both core and rim giving Archaean ages of *ca.* 2900  
370 Ma). The analyses are generally low in U and the Th/U ratios range to very high values (0.16–  
371 4.06), apart from those of grains #10 and #11 (0.08). The analyses mostly plot on a simple  
372 discordia between  $1892 \pm 62$  Ma and  $973 \pm 82$  Ma (MSWD rather high at 2.4). There are a  
373 number of discordant analyses, but these do not indicate the presence of intermediate

374 Mesoproterozoic zircon. The three youngest Grenvillian areas are highly concordant and yield  
375 a defined Concordia age of  $940 \pm 6$  Ma (MSWD = 0.004), which is taken as the best age for the  
376 Pb-loss and possible metamorphic event. There is a possibility that this rock underwent an  
377 older thermal event responsible for the Paleoproterozoic ages of some overgrowths. The  
378 ultimate age of the protolith is unknown as insufficient data were obtained from cores.

380 *ILO-19*. Mylonitic porphyritic granite (Fig. 5a). The abundant zircons in this sample are  
381 elongate, mostly  $\sim 200$   $\mu\text{m}$  in length, or longer, with either subround or pyramidal  
382 terminations. Many grains can be seen to be strongly zoned under transmitted light and  
383 although many are clear and colourless a few are dark and metamict. CL shows a variety of  
384 internal structures. Many grains and areas within grains are simple oscillatory zoned zircon,  
385 but there are prominent grains with very irregular internal features and in places these wispy  
386 features overprint and cross-cut what is interpreted to be the primary simple igneous zoning.

387  
388 Twenty-three areas were analysed on 20 grains covering the full range of complex internal  
389 CL structures. All 23 analyses yield  $^{206}\text{Pb}/^{238}\text{U}$  ages in the range 415–465 Ma and the relative  
390 probability plot shows a broad peak or peaks centred at about 450 Ma. Apart from 3 analyses  
391 (#3, #4.1 & #15) the data are low in common Pb and the  $^{204}\text{Pb}$ -corrected data are within  
392 uncertainty of concordia. There is no evidence for any Grenville-age event in these zircon  
393 grains. There is a wide range in U and Th contents, but the Th/U ratios are moderate to high,  
394 reflecting the dominantly igneous nature of the zoned zircon. If the three analyses with high  
395 common Pb and all others with  $>10\%$  discordance are excluded, three possible age peaks can  
396 be recognized: *ca.* 460 Ma, *ca.* 446 Ma and *ca.* 432. The younger peak could be related to  
397 retrogression within the shear zone (overprinting features in zircon grains) which is strong in



398 this rock.

399

400 *ILO-20*. Dark mylonitic gneiss (Fig. 5b). The zircons from this sample are mostly slender,  
401 elongate grains with subhedral terminations. More equant and bulkier elongate grains are also  
402 present, tending to be coarser-grained, up to 250µm in length and 50µm in width. The CL  
403 images show a complex internal structure. Whilst many grains have length-parallel zoning  
404 (interpreted as igneous), more homogeneous, possibly metamorphic, zircon is present both as  
405 rims and in places forming anastomosing embayments into the zoned igneous zircon.

406

407 Twenty-six areas were analysed on 21 grains ( Fig. 5b). A wide range of the internal  
408 structures noted above were analysed, with both the zoned igneous and the more  
409 homogeneous areas interpreted as metamorphic analysed on a number of single grains. The  
410 resulting data form a dispersed grouping that is dominantly within uncertainty of the Tera-  
411 Wasserburg Concordia. Two analyses, #2.2 and #6.1, are more enriched in common Pb; the  
412 former yields a young  $^{206}\text{Pb}/^{238}\text{U}$  date of *ca.* 438 Ma and the area analysed is considered to  
413 have lost radiogenic Pb. The relative probability plot of  $^{206}\text{Pb}/^{238}\text{U}$  ages shows a dominant  
414 bell-shaped peak, which yields a weighted mean age of  $464\pm 4$  (MSWD = 1.07). It is  
415 noteworthy that this grouping includes both zoned igneous and the more homogeneous zircon  
416 areas; thus the igneous emplacement and subsequent metamorphic developments in these  
417 grains occurred within the analytical uncertainty of 464 Ma. On the older age side, there is a  
418 subordinate grouping around *ca.* 480 Ma (four analyses give a mean of  $483\pm 7$  Ma) and  
419 scattered older dates to *ca.* 512 Ma. The central areas to a number of grains were analysed as  
420 it was originally presumed that this rock would yield a Grenvillian age. However, whilst  
421 there are scattered analyses older than the dominant Ordovician peak, there is no evidence for  
422 such a Grenville event.

423

1  
2 424 *ILO-23*. Anorthosite (Fig. 5c). Only a few zircon grains were separated from this sample (7  
3  
4  
5 425 on the probe mount). They are elongate and range from clear subhedral forms to dark,  
6  
7 426 metamict subhedral grains. The CL images are very dark, but relict igneous zoning can be  
8  
9 427 seen.

10  
11 428

12  
13  
14 429 Seven areas were analysed on 6 grains; they have high U ranging from 1700 to 3065 ppm,  
15  
16  
17 430 with relatively moderate Th and Th/U ratios in the range 0.08 –0.21. This is on the slightly  
18  
19 431 low side for normal igneous zircon but may reflect late-stage magmatic crystallisation or  
20  
21  
22 432 partial melting. The areas analysed are low in common Pb, but not ideal in terms of zircon  
23  
24 433 clarity or good CL structure. The relative probability plot for the limited number of analyses  
25  
26  
27 434 is irregular, with one clearly older analysis and some skew to the young age side. A weighted  
28  
29 435 mean of the  $^{206}\text{Pb}/^{238}\text{U}$  ages for 5 of the 7 analyses provides an estimated crystallisation date  
30  
31 436 of  $464\pm 5$  Ma (MSWD = 1.0).

32  
33  
34 437

35  
36 438

37  
38  
39 439 **Pegmatites**

40  
41 440

42  
43 441 Because Rb is strongly fractionated in muscovite relative to Sr, the  $^{87}\text{Sr}/^{86}\text{Sr}$  ratio in the  
44  
45  
46 442 mineral increases very quickly time and the calculated age is insensitive to the assumed initial  
47  
48  
49 443 values for calc-alkaline magmas. The ages of two muscovite samples obtained in this way  
50  
51 444 were 1000 and 1100 Ma (Table 3), i.e., Grenvillian. These pegmatites, although roughly  
52  
53 445 concordant to their host rocks, do not show evidence for ductile deformation and/or  
54  
55  
56 446 superimposed metamorphism, and the Rb-Sr ages are taken as dating magmatic  
57  
58 447 crystallization.

59  
60  
61  
62  
63  
64  
65

448

1

2 449

3

4

5 450

## **REE and Nd isotope data**

6

7 451

8

9 452

REE data for five samples of high-grade gneisses from the Camaná–Mollendo domain

10

11 453

(Table 4) are plotted in Fig. 6. They show enrichment in LREE relative to HREE, with

12

13 454

(La/Yb)<sub>N</sub> values between 13.5 and 24, and a small negative Eu anomaly ( $Eu/Eu^* = ca. 0.8$ ).

14

15 455

REEs patterns are remarkably similar in the five gneisses suggesting that they were all

16

17 456

derived from the same type of protolith. They are also strikingly similar to those of shales,

18

19 457

e.g., the North American Shale Composite (Taylor and McLennan, 1988), so that it may be

20

21 458

inferred that the gneisses were derived from detrital sedimentary rocks. The small differences

22

23 459

among the five rocks analysed here may be attributed to variable melt extraction during

24

25 460

migmatization.

26

27 461

28

29 462

Nd isotope composition is available for the five high-grade gneisses (Table 2). They

30

31 463

yielded  $\epsilon_{Nd}$  values of -5.5 to -8.2 at the reference age of 1700 Ma. Nd single-stage depleted-

32

33 464

mantle model ages ( $T_{DM}$ , DePaolo et al. 1981) range between *ca.* 2.3 and 2.5 Ga.

34

35 465

36

37 466

Nd isotope composition is also available for three meta-igneous rocks from the Ilo domain.

38

39 467

$\epsilon_{Nd}$  values at the reference age of 475 Ma (Table 2) differ significantly from one rock to

40

41 468

another: -6.4 (ILO-19), -7.8 (ILO-20) and -3.6 (ILO-23), the latter being for the anorthosite.

42

43 469

The value for ILO-20, the mafic gneiss, is less primitive than that of the granite, perhaps

44

45 470

indicating different protoliths and not only strain differences between the two rocks as might

46

47 471

be argued from field evidence alone.

48

49 472

50

51 473

52

53 474

54

55 475

56

57 476

58

59 477

60

61 478

62

63 479

64

65

473 **Discussion**

474

475 Two views emerge from these data. 1) The geological history of the Arequipa massif  
476 covers a very long period of time, between Paleoproterozoic and Early Paleozoic  
477 (Ordovician–Silurian). 2) Three main rock-forming events took place, at widely separated  
478 times: in the Paleoproterozoic, in the Late Mesoproterozoic and in the Paleozoic.

479

480 The Paleoproterozoic. An old orogenic history

481

482 The protolith of the strongly retrogressed quartzose gneiss MAR-8 from the San Juan  
483 Marcona domain was a felsic igneous rock, probably volcanic or subvolcanic. Its age of  
484  $1796 \pm 13$  Ma (Late Paleoproterozoic) coincides with a discordia upper intercept age of  
485  $1793 \pm 6$  Ma found by Loewy et al. (2004) for a retrogressed foliated megacrystic granite  
486 nearby (sample U/Pb-3). The age of *ca.* 1.79 Ga thus corresponds to an event of felsic  
487 magmatism. Moreover, this age constrains the age of the host metasedimentary rocks that  
488 were coeval or older.

489

490 Migmatitic gneisses of the Camaná–Mollendo domain, although separated from the San  
491 Juan domain by the Atico medium-grade rocks and the Ocoña Phyllonite zone, probably  
492 correspond to the same geological domain, although they are generally less retrogressed and  
493 appear to contain material older than the igneous protolith in the San Juan Marcona domain.  
494 Most of the migmatitic gneisses are probably metasedimentary, as inferred from both the  
495 similarity of their REE pattern to those of shales and the high peraluminosity evidenced by  
496 the mineral compositions (Martignole & Martelat, 2003).

497

498 All the samples contain Paleoproterozoic zircons that underwent a metamorphic overprint  
1  
2 499 of Grenvillian age. Low-discordance Paleoproterozoic ages range from 1.76 to 2.1 Ga. A few  
3  
4 500 scattered Archaean zircons were also found (*ca.* 2.7 Ga in CAM-7, *ca.* 2.9 Ga in MOL-17).  
5  
6  
7 501 Moreover, the Paleoproterozoic ages embrace detrital cores with relict igneous zoning and  
8  
9 502 thick subrounded, homogeneous or weakly concentrically-zoned, overgrowths (mantles). The  
10  
11 503 latter features are common in high-grade metamorphic zircons (Vavra et al., 1999; Corfu et  
12  
13 504 al., 2003). Most of the analysed areas were overgrowths, most of them with Th/U values  
14  
15 505 higher than most metamorphic zircons (which tend to have values  $< 0.1$ ). This fact however  
16  
17 506 has been also recognized in other high-grade metamorphic areas (e.g., Goodge et al., 2001)  
18  
19 507 and, of particular relevance, in UHT metamorphic regions, e.g., in the Napier Complex,  
20  
21  
22 508 Antarctica (Carson et al., 2002). Such high Th/U values in metamorphic mantles are attributed  
23  
24 509 to U-depletion during UHT metamorphism prior to zircon growth (Black et al., 1986; Carson  
25  
26 510 et al., 2002). We propose that the zircon overgrowths in the Arequipa massif migmatitic  
27  
28 511 gneisses probably resulted from UHT metamorphism in the Paleoproterozoic.  
29  
30  
31  
32  
33

34 512  
35  
36 513 Samples CAM-2 and CAM-7 contain detrital igneous cores of 1890 Ma to 2080 Ma that,  
37  
38 514 along with the few Archaean cores referred to above, suggest magmatic events in the source  
39  
40 515 area of the sedimentary protoliths in the Middle Paleoproterozoic (Rhyacian and Orosirian)  
41  
42 516 and in the Archaean. Most of the analysed zircon areas plot on discordias resulting from Pb-  
43  
44 517 loss during Grenvillian metamorphism, and as most correspond to mantles on older cores, the  
45  
46 518 upper intercept ages probably date metamorphism. The strongest cases are for samples QUI-  
47  
48 519 16 and MOL-17, where only overgrowths were considered for regression; the resulting ages  
49  
50 520 are  $1861 \pm 32$  Ma and  $1892 \pm 62$  Ma, respectively. Thus a metamorphic event at *ca.* 1.87 Ga is  
51  
52 521 inferred for the Paleoproterozoic overgrowths. Whether these Paleoproterozoic overgrowths  
53  
54 522 formed *in situ* or were detrital is more difficult to assess. Zircon grains in samples QUI-16  
55  
56  
57  
58  
59  
60  
61  
62  
63  
64  
65

523 and MOL-17 show overgrowths that are quite regular and complete around detrital igneous  
524 cores (Fig. 4). This might be taken as compatible with overgrowth formation *in situ* and  
525 consequently with a metamorphic event in the Camaná-Mollendo domain at *ca.* 1.87 Ga. This  
526 interpretation strengthens that of Loewy et al. (2004), who argued on geological grounds for a  
527 metamorphic event (M1) and deformation at *ca.* 1.8 Ga, i.e., prior to the intrusion of the  
528 megacrystic granite (U/Pb3). Consequently, the age of the sedimentary protoliths of the  
529 migmatitic gneisses can now be bracketed with some confidence between *ca.* 1.87 and the  
530 minimum age of detrital igneous zircons, i.e., *ca.* 1.9 Ga. In consequence sedimentary  
531 protoliths formed shortly before metamorphism. Quite similarly Cobbing et al. (1977),  
532 Dalmayrac et al.(1977) and Shackleton et al. (1979) argued in favour of a granulite facies  
533 regional metamorphism between *ca.* 1.8 and 1.95 Ma, with protolith ages of *ca.* 2000 Ma.  
534 However these authors considered that the granulitic gneisses resulted from a single  
535 metamorphic event and did not recognize the superimposed Grenvillian event (see below).

536

537 Nd isotope values ( $T_{DM}$  between *ca.* 2.3 and 2.55 Ga) suggest that Nd in the Camaná-  
538 Mollendo migmatitic gneisses is largely reworked from an old continental crustal material,  
539 Paleoproterozoic and/or Archaean. This is compatible with the presence in some samples of  
540 old detrital zircons of *ca.* 2690 Ma (CAM-7) and *ca.* 2900 Ma (MOL-17) that indicate an  
541 Archaean source. Moreover, the crustal source of the zircons experienced magmatism at  
542 different times between *ca.* 1.9 and 2.1 Ga, probably with addition of a juvenile component to  
543 the upper continental crust. This constitutes a significant fingerprint of the source area, i.e.,  
544 old Nd model ages and a younger zircon population.

545

546 As for the Paleoproterozoic, the pattern that emerges from zircon ages and the geological  
547 and geochemical evidence is one of an orogeny between *ca.* 1.79 and 2.1 Ga (Orosirian to

1 548 Rhyacian) involving: a) early magmatism (between 1.89 and 2.1Ga), presumably through  
2 549 partly Archaean continental crust, b) sedimentation of a thick sequence of terrigenous  
3  
4 550 sediments, c) UHT metamorphism at *ca.* 1.87 Ga, and d) late felsic magmatism at *ca.* 1.79  
5  
6  
7 551 Ga.  
8

9 552

10  
11  
12 553 The Atico domain: a Mesoproterozoic sedimentary basin.  
13

14 554

15  
16  
17 555 The only sample from this medium-grade metamorphic domain (OCO-26) shows  
18  
19 556 similarities to the migmatitic gneisses of the Camaná–Mollendo domain, but also significant  
20  
21 557 differences. Many low-discordance areas yield ages between 1700 and 2030 Ma and a few are  
22  
23  
24 558 Archaean, between 2600 and 2800 Ma (one discordant age *ca.* 3100 Ma). These ages are from  
25  
26 559 detrital igneous cores and metamorphic mantles, and are similar to the Proterozoic to  
27  
28  
29 560 Archaean low-discordance ages found in the Camaná–Mollendo and San Juan domains. On  
30  
31 561 the other hand, OCO-26 contains zircons with nearly concordant ages between *ca.* 1200 and  
32  
33  
34 562 *ca.* 1600 Ma. This group of ages has not been recognized in the high-grade domains; we  
35  
36 563 interpret these zircons as detrital. Grenvillian metamorphism started at *ca.* 1000 Ma.  
37

38  
39 564

40  
41 565 Deposition of the sedimentary protolith of OCO-26 occurred between *ca.* 1200 and  
42  
43 566 *ca.*1000 Ma, i.e., in the Late Mesoproterozoic. Detrital zircons were fed from a source area  
44  
45  
46 567 similar to the high-grade Camaná–Mollendo and San Juan domains, but also from an  
47  
48 568 unknown source that provided the Mesoproterozoic zircons of 1200–1600 Ma. The Atico  
49  
50  
51 569 domain can thus be interpreted as a sedimentary basin deposited on a Paleoproterozoic high-  
52  
53 570 grade basement consisting of igneous and metamorphic rocks. Cobbing et al. (1977) first  
54  
55  
56 571 considered the Atico metasedimentary rocks to be younger than the Mollendo high-grade  
57  
58  
59  
60  
61  
62  
63  
64  
65

572 gneisses because of the presence of quartzites, absent in Camaná–Mollendo domain. However  
1  
2 573 this opinion was challenged by Wasteneys et al. (1995).

3  
4  
5 574

6  
7 575 The Grenville-age metamorphic event  
8

9  
10 576

11 All the zircon populations from the San Juan, Atico and Camaná-Mollendo samples show

12 577 the imprint of a metamorphic event Late-Mesoproterozoic to Early Neoproterozoic in age.  
13

14 578 This metamorphism produced Pb-loss on both older zircon igneous cores and on  
15  
16 579 Paleoproterozoic overgrowths, giving rise to linear discordias, and probably new overgrowths

17 580 in the form of contrasting luminescence rims. Recorded Grenvillian ages can be bracketed  
18  
19 581 between *ca.* 940 and *ca.* 1080 Ma, taking age uncertainties into account. In the Camaná-

20 582 Mollendo domain Grenvillian ages are apparently older in the Quilca and Camaná samples  
21  
22 583 (CAM-2: 1040±11 Ma; CAM-7: 1026±32 Ma; QUI-16: 1011±73 Ma) than in the Mollendo

23 584 sample (MOL-17: 940±6 Ma), a fact that was also recognized by Wasteneys et al. (1995;

24 585 point C: 966±5 Ma) and by Loewy et al. (2004; sample U/Pb-2: 935±14 Ma). Sample MAR-8  
25  
26 586 from the San Juan Marcona domain yielded an age of 1033±23 Ma for the Grenvillian event,  
27  
28 587 i.e., within error of those of the southern Camaná-Mollendo domain. The weighted average  
29  
30 588 age of metamorphism in northern Camaná–Mollendo and San Juan Marcona is 1037±19 Ma.

31 589 In the Atico domain we found a spread of Grenvillian ages between *ca.* 1000 and *ca.* 840 Ma.  
32  
33 590 The latter domain underwent only Grenvillian metamorphism, in contrast with the Camaná–

34 591 Mollendo domain, which besides Grenvillian metamorphism underwent an older  
35  
36 592 Paleoproterozoic event. Martignole and Martelat (2003) carried out chemical dating of  
37  
38 593 monazites from the Camaná–Mollendo domain and found a spread of Grenvillian ages;  
39  
40 594 statistically meaningful ages of *ca.* 1000 Ma were obtained for three samples near Camaná.

41 595 Moreover, muscovite pegmatites, probably migmatitic melts, were emplaced during the  
42  
43 596  
44  
45  
46  
47  
48  
49  
50  
51  
52  
53  
54  
55  
56  
57  
58  
59  
60  
61  
62  
63  
64  
65



597 Grenvillian event (1000 and 1100 Ma) as inferred from the Sr isotope composition of  
1  
2 598 muscovites presented here.  
3

4 599  
5  
6  
7 600 Grenville-age metamorphism at Arequipa took thus place in as many as three separate  
8  
9 601 episodes: 1) *ca.* 1040 Ma in the Quilca and Camaná areas of the Camaná–Mollendo domain,  
10  
11 602 and in the San Juan Marcona domain, 2) at 940±6 Ma in the Mollendo area of the Camaná–  
12  
13 603 Mollendo domain; 3) between *ca.* 1000 and 840 Ma in the Atico domain. This evidence  
14  
15 604 suggests that in the Arequipa massif metamorphic domains are juxtaposed that underwent  
16  
17 605 Grenvillian metamorphism at different times and had different cooling histories.  
18  
19  
20  
21

22 606  
23  
24 607 It is difficult to distinguish the effects of the Grenvillian metamorphic overprint on the  
25  
26 608 older UHT paragenesis. Martignole & Martelat (2003), although favouring a single  
27  
28 609 metamorphism of Grenville-age, leave this question open, suggesting that this might  
29  
30 610 correspond to the lowest-P event ( $T < 900^{\circ}\text{C}$ ) they recognized. In our hypothesis that the UHT  
31  
32 611 metamorphism in Arequipa was Paleoproterozoic, temperatures attained during Grenvillian  
33  
34 612 metamorphism had to be high enough to completely reset the Th-U-Pb system in monazites  
35  
36 613 (*ca.* 730°C; Copeland et al., 1988; Parrish, 1990) unless the monazite formed only during the  
37  
38 614 Grenvillian event. Moreover Grenville-age Ms-pegmatites are evidence for renewed partial  
39  
40 615 melting at this time. Temperatures between 730° and 900°C were thus probably attained  
41  
42 616 during Grenvillian metamorphism in the Camaná–Mollendo domain. In the Atico domain  
43  
44 617 however, Grenvillian metamorphism only attained P-T values within the stability field of  
45  
46 618 staurolite+andalusite (Shackleton et al., 1979) implying a low-pressure type of  
47  
48 619 metamorphism.  
49  
50  
51  
52

53 620  
54  
55  
56 621 Paleozoic events: the Ordovician magmatic arc  
57  
58  
59  
60  
61  
62  
63  
64  
65

622

1  
2 623 Ordovician crystallization ages found here for the igneous protoliths of the Ilo domain  
3  
4  
5 624 were unexpected. Martignole et al. (2005) interpreted these rocks as a Grenvillian AMG  
6  
7 625 (anorthosite-mangerite-charnockite-granite) suite on the basis of locally preserved relict high-  
8  
9 626 temperature minerals such as pyroxenes and alleged metamorphic garnet, and Nd model ages  
10  
11 627 of *ca.* 1.15 Ga. In our samples those minerals are absent. However minerals such as  
12  
13 628 hornblende, biotite and rutile (in anorthosite) are preserved in the less retrogressed rocks  
14  
15 629 (ILO-20 and ILO-23) and also argue in favour of an earlier high-temperature history  
16  
17 630 including igneous crystallization in a deep magma chamber and metamorphism. The latter,  
18  
19 631 which is evidenced by zircon overgrowths on igneous cores (e.g., ILO-20), took place within  
20  
21 632 the analytical uncertainty of the crystallization ages. Ages of igneous zircons of *ca.* 460 Ma  
22  
23 633 place this magmatism within the Famatinian orogenic cycle, well-known in NW Argentina,  
24  
25 634 which took place along the proto-Andean margin of Gondwana (Pankhurst et al., 2000;  
26  
27 635 Dahlquist et al., 2008, and references therein). Loewy et al. (2004) obtained U-Pb ages  
28  
29 636 between 440 and 468 Ma for late granitic intrusions in the Arequipa massif. Nd isotope  
30  
31 637 considerations suggest that the Ilo magmatism involved variable contamination with an  
32  
33 638 evolved continental crust ( $\epsilon\text{Nd} = -3.6$  to  $-7.8$ ;  $T_{\text{DM}} = 1.5$  to  $1.8$  Ga) with some evidence for  
34  
35 639 mixing/mingling between magmas.  
36  
37  
38  
39  
40  
41  
42  
43

640

44  
45 641 A Paleozoic metamorphic event is also recorded in the San Juan Marcona domain. Here  
46  
47 642 (sample MAR-8), an event that produced variable Pb-loss of Grenvillian and Paleoproterozoic  
48  
49 643 zircon is suggested by a discordia with a lower intercept at  $469 \pm 70$  Ma. Strong retrogression  
50  
51 644 in the San Juan Marcona and Ocoña areas was attributed by Loewy et al. (2004) to an M3  
52  
53 645 tectonothermal event at *ca.* 465 Ma, i.e., Ordovician, as inferred from the U-Pb ages of  
54  
55 646 alleged pre- and post-metamorphic plutons in the area. This event correlates with the  
56  
57  
58  
59  
60  
61  
62  
63  
64  
65

647 Marcona event of Shackleton et al. (1979), which produced a foliation (S3) and greenschist-  
648 facies retrogression of the basement gneisses. The Ocoña phyllonite zone that separates the  
649 Atico domain from the Camaná–Mollendo domain was attributed to this M3-S3 event  
650 (Shackleton et al., 1979; Loewy et al., 2004).

651  
652 In the Ilo domain, zircons from the mylonitic dark gneiss and mylonitic porphyritic granite  
653 record evidence of overprinting at 430–440 Ma that could be related to retrogression within  
654 the shear zone. This age is within error of that found at San Juan Marcona and attests to  
655 metamorphic processes in Ordovician to Silurian times. This Ordovician to Silurian low-grade  
656 metamorphic overprint was largely restricted to shear zones and basement areas near the  
657 contact with cover sequences of Neoproterozoic age, such as in the San Juan Marcona domain  
658 (Shackleton et al., 1979; Chew et al., 2007). Focused flow of water-rich fluids along these  
659 zones played a significant role in metamorphism. Large areas of the Arequipa massif,  
660 however, do not record any evidence of Paleozoic metamorphism.

661

### 662 Correlations and geodynamic implications

663

664 There is agreement that the Laurentia and Amazonia cratons were juxtaposed across the  
665 Grenvillian orogenic belt at the end of Rodinia amalgamation at *ca.* 1.0 Ga (e.g., Dalziel,  
666 1997; Davidson, 1995; Loewy et al., 2003; Tohver et al., 2004; Li et al., 2008). Models differ  
667 however on the relative position of these cratons, either in the NE (relative to present-day  
668 North America) or in the SE. Fig. 7 shows a paleomagnetically-constrained paleogeography at  
669 *ca.* 1.2 Ga, i.e., the alleged age of collision, according to Tohver et al. (2004). It shows the  
670 location of the Grenville belt of North America and its alleged counterpart along the western

1  
2 672 and southwestern margin of Amazonia, together with outcrops of basement in the central  
3 Andes region with Grenvillian ages of interest to this contribution.

4  
5 673  
6  
7 674 The Arequipa massif is a Paleoproterozoic inlier overprinted by the Grenvillian orogeny.  
8  
9 675 Correlation with other Paleoproterozoic terranes in Laurentia or Amazonia is hindered by the  
10 isolation of the Arequipa massif. Compared with the ages of Paleoproterozoic orogenies in  
11  
12 676 Laurentia (e.g., Goodge & Vervoort, 2006, fig. 1; Goodge et al., 2004, fig. 16) the age interval  
13  
14 677 1.76–2.1 Ga of Paleoproterozoic zircon in the San Juan and Camaná–Mollendo domains  
15  
16 678 embraces the Yavapai orogeny (1.7–1.8 Ga) and the Penokean and Trans-Hudson orogenies  
17  
18 679 (1.8–2.0 Ga; Schulz & Cannon, 2007; Whitmayer and Karlstrom, 2007). If formerly part of  
19  
20 680 Laurentia, the Arequipa massif would be a relic of the pre-Grenvillian southern margin of the  
21  
22 681 continent (present coordinates) isolated from the northern Paleoproterozoic belts by younger  
23  
24 682 juvenile accretionary belts (Mazatzal and the Granite-Rhyolite province: 1.7–1.3 Ga; Fig. 7).  
25  
26 683 The Laurentian connection was favoured by Wasteneys et al. (1995) and Loewy et al. (2003,  
27  
28 684 2004). On the other hand, rocks equivalent in age are also found in the Venturi–Tapajós belt  
29  
30 685 of the Amazonia craton (2.0–1.8 Ga; Cordani and Teixeira, 2007). Nevertheless, the latter is a  
31  
32 686 juvenile accretionary belt whilst the Arequipa massif is a block of reworked continental crust.  
33  
34 687 Moreover the Venturi–Tapajós belt is quite distant from the Arequipa massif even in current  
35  
36 688 reconstructions, which would imply a significant lateral displacement before Grenvillian  
37  
38 689 metamorphism.  
39  
40 690

41  
42 691  
43  
44  
45  
46  
47  
48  
49  
50  
51 692 The Rio Apa block, south of present day Amazonia (Fig. 7), is another area to be  
52  
53 693 considered, with U-Pb SHRIMP zircon ages largely coincident with those of detrital zircons  
54  
55 694 in the Arequipa migmatitic gneisses (Cordani et al., 2008). Here widespread granitoid  
56  
57 695 gneisses (1.94 Ga) were intruded by granitic plutons of the Alumiador Intrusive Suite (*ca.*  
58  
59  
60  
61  
62  
63  
64  
65

696 1.83 Ga) and younger orthogneisses between 1.7 and 1.76 Ga. Nd model ages are between 2.2  
697 and 2.53 Ga (Cordani et al., 2005). Allegedly Paleoproterozoic metamorphism was medium-  
698 to high-grade (Cordani et al., 2008), but so far no evidence of UHT metamorphism has been  
699 recorded. The Rio Apa block was overprinted by a Grenville-age thermal event between *ca.*  
700 1.3 and 1.0 Ga (Cordani et al., 2005) and with the Arequipa massif could thus be part of a  
701 larger Paleoproterozoic inlier within the South American counterpart of the Grenville orogen.  
702 The Maz domain in the Western Sierras Pampeanas of Argentina contains metasedimentary  
703 rocks with Paleoproterozoic zircons (1.7–1.9 Ga) and old Nd model ages (1.7–2.7 Ga), and  
704 was also reworked by the Grenvillian orogeny (Casquet et al., 2008), so that it could also be  
705 part of the same continental block.

706  
707 Accretion of the Arequipa massif to Amazonia has been attributed to the Grenvillian  
708 (Sunsás) orogeny (Wasteneys et al., 1995; Loewy et al., 2004). Grenvillian ages of igneous  
709 rocks and metamorphism were early recognized along the southeastern margin of the  
710 Amazonia craton by Priem (1971) and Lintherland et al. (1989). The latter coined the name  
711 Sunsás orogeny for this tectonothermal event and attributed to it an age of *ca.* 1000 Ma.  
712 Orogeny involved folding and metamorphism along discrete metasedimentary belts that wrap  
713 around an older metamorphic core, the Rondonian–San Ignacio province (1.5–1.3 Ga;  
714 Cordani and Teixeira, 2007). Tohver et al. (2004) summarized the Grenvillian history as  
715 consisting of two events, an older one of Laurentia–Amazonia collision (1.2–1.12 Ga), and a  
716 younger one of alleged oblique convergence and intracontinental strike-slip at *ca.* 1.1  
717 (Sunsás–Aguapei–Nova Brasilândia orogeny). The second event was accompanied by  
718 magmatism and metamorphism within the metasedimentary belts. Metamorphism was mostly  
719 of low grade but also reached granulitic facies (at Nova Brasilândia), dated at 1.09 Ga with  
720 cooling through 920 Ma. Precise U-Pb SHRIMP ages led Boger et al. (2005) to constrain

1  
2  
3  
4  
5  
6  
7  
8  
9  
10  
11  
12  
13  
14  
15  
16  
17  
18  
19  
20  
21  
22  
23  
24  
25  
26  
27  
28  
29  
30  
31  
32  
33  
34  
35  
36  
37  
38  
39  
40  
41  
42  
43  
44  
45  
46  
47  
48  
49  
50  
51  
52  
53  
54  
55  
56  
57  
58  
59  
60  
61  
62  
63  
64  
65

721 Sunsás deformation as predating *ca.* 1070 Ma. Santos et al. (2008) revisited the tectonic  
722 evolution of the southern margin of Amazonia and re-interpreted the Sunsás orogeny as an  
723 autochthonous orogen involving four orogenic pulses between 1465 and 1110 Ma, suggesting  
724 a Laurentia–Amazonia connection at *ca.* 1450 Ma. The period between 1070 Ma and *ca.* 980  
725 Ma was apparently a period of craton stabilization, with anorogenic granitic magmatism along  
726 the southern margin of Amazonia (Santos et al., 2008; Cordani and Teixeira, 2007, and  
727 references therein).

728  
729 In the Grenville province of Canada the Grenvillian orogenic cycle started at *ca.* 1.25 Ga  
730 and ended at *ca.* 850 Ma (Davidson, 1995, Rivers, 1997). Between 1100 and *ca.* 980 Ma, the  
731 orogenic cycle involved two contractional episodes: the widespread penetrative Ottawa  
732 orogeny (1080–1020 Ma) and the more localized Rigolet event (1000–980 Ma). In a recent  
733 interpretation of the crustal-scale orogenic evolution of the Grenville province, Rivers (2008)  
734 argued that collapse of the Ottawa thickened orogen took place during the time interval  
735 1050–1020. Former contractional structures were reworked in extension and AMG  
736 complexes were intruded that heated the middle crust. Horst-and-graben structures developed  
737 at this time in the upper crust. During the time interval 1020–950 Ma the Grenville province  
738 underwent contraction at the Grenville front. The hinterland however underwent protracted  
739 extensional collapse over this period with development of extensional shear zones, deep  
740 ductile detachments and metamorphism (Rivers, 2008).

741  
742 The contractional phase of the Ottawa orogeny (1080–1050 Ma) and the older Grenvillian  
743 orogenic cycle events are not recognized in the Arequipa massif. However, the coincidence of  
744 the Arequipa massif Grenvillian metamorphic ages of 1040–840 Ma with protracted extension  
745 both in the Laurentian Grenville orogen (except for the localized Rigolet pulse at *ca.* 1.0 Ga)

1  
2  
3  
4  
5  
6  
7  
8  
9  
10  
11  
12  
13  
14  
15  
16  
17  
18  
19  
20  
21  
22  
23  
24  
25  
26  
27  
28  
29  
30  
31  
32  
33  
34  
35  
36  
37  
38  
39  
40  
41  
42  
43  
44  
45  
46  
47  
48  
49  
50  
51  
52  
53  
54  
55  
56  
57  
58  
59  
60  
61  
62  
63  
64  
65

746 and in southern Amazonia suggests that metamorphism in Arequipa, which was low-P type,  
747 might be related to overall extension and heating, and not to collision as formerly argued. The  
748 precise tectonic setting remains unknown and more structural work is required to constrain it.  
749 Laurentia–Amazonia collision took probably place earlier, at *ca.* 1.2 Ga (Tohver et al., 2004)  
750 or during the Ottawa orogeny (Rivers, 1977, 2008) but is not recognized in the Arequipa  
751 massif except for the detrital zircons of 1200–1260 Ma in the Atico metasedimentary rocks.  
752 Whether formerly part of Laurentia or of Amazonia, the location of Arequipa before collision  
753 remains uncertain.

754  
755       The Atico sedimentary basin that formed between 1200 and 1000 Ma might be also  
756 related to the protracted extensional event referred to above. The magmatism at Ilo that  
757 included anorthosites was not involved in the Grenvillian metamorphism. Grenvillian  
758 metamorphic domains with different P-T-t histories were probably juxtaposed across low-  
759 grade shear zones in the Ordovician–Silurian.

760

761

## 762 **Conclusions**

763

764       The Arequipa massif is a Paleoproterozoic inlier in the South American Grenville-age  
765 orogen. It was probably part of a larger continental block that also included the Río Apa block  
766 and the western Sierras Pampeanas Maz terrane.

767

768       The Paleoproterozoic pattern that emerges is one of an orogeny between *ca.* 1.79 and 2.1  
769 Ga (Orosirian to Rhyacian) involving: a) early magmatism (between 1.89 and 2.1Ga),  
770 presumably through partly Archaean continental crust, b) sedimentation of a thick sequence

771 of terrigenous sediments, c) UHT metamorphism at *ca.* 1.87 Ga, and d) late felsic magmatism  
772 at *ca.* 1.79 Ga.

773  
774 The Atico domain can be interpreted as a sedimentary basin deposited on a  
775 Paleoproterozoic high-grade basement consisting of igneous and metamorphic rocks.  
776 Deposition occurred between *ca.* 1200 and *ca.* 1000 Ma, i.e., in the Late Mesoproterozoic.  
777 Detrital zircons were derived from a source area similar to the high-grade Camaná–Mollendo and  
778 San Juan domains, but also from an unknown source that provided Mesoproterozoic zircons  
779 of 1260–1600 Ma.

780  
781 Grenville-age metamorphism at Arequipa took place in up to three stages: 1) *ca.* 1040 Ma  
782 in the Quilca and Camaná areas of the Camaná–Mollendo domain, and in the San Juan  
783 Marcona domain, 2) 940±6 Ma in the Mollendo area of the Camaná–Mollendo domain; 3)  
784 between 1000 and 850 Ma in the Atico domain. In the Arequipa massif metamorphic domains  
785 are therefore juxtaposed that underwent different Grenvillian metamorphic histories. The  
786 geodynamic significance of Grenvillian metamorphism is unknown but it could be related to  
787 extension and not to collision as formerly argued.

788  
789 During the early Paleozoic the Arequipa massif underwent magmatism at *ca.* 465 Ma and  
790 focused retrogression along shear zones or unconformities between 430 and 440 Ma.

791

## 792 **Acknowledgements**

793  
794 Financial support for this work was provided by Spanish MEC grant CGL2005-  
795 02065/BTE and Universidad Complutense grant 910495 and Argentinian PICT 1009. We are



796 grateful to Instituto Geológico Minero y Metalúrgico (INGEMMET) of Perú, and particularly  
797 to Dr. Victor Carlotto, who helped us with the fieldwork.

798

799

## 800 **References**

801

802 Arima, M, and Gower, Ch.F., 1991. Osumilite-bearing granulites in the eastern Grenville

803 Province, Eastern Labrador, Canada: Mineral parageneses and metamorphic conditions.

804 Journal of Petrology, 32, 1, 29-61.

805 Black L.P., Williams, I.S., Compston, W., 1986. Four zircon ages from one rock: the history

806 of a 3930 Ma old granulite from the Mt. Stones, Enderby Land, Antarctica. Contributions

807 to Mineralogy and Petrology, 94, 427-437.

808 Bock, B., Bahlburg, H., Wörner, G., Zimmerman, U., 2000. Tracing crustal evolution in the

809 Southern Central Andes from Late Precambrian to Permian with geochemical and Nd and

810 Pb data. Journal of Geology, 108, 515-535.

811 Boger, S.D., Raetz, M., Giles, D., Etchart, E., Fanning, C.M., 2005. U-Pb data from the

812 Sunsas region of Eastern Bolivia, evidence for an allocthonous origin of the Paragua block.

813 Precambrian Research, 139, 121-146.

814 Carson, C.J., Ague, J.J., Coath, C.D., 2002. U-Pb geochronology from Tonagh Island, East

815 Antarctica: Implications from the timing of ultra-high temperature metamorphism of the

816 Napier Complex. Precambrian Research, 116, 237-263.

817 Casquet, C., Pankhurst, R.J., Rapela, C., Galindo, C., Fanning, C.M., Chiaradia, M., Baldo,

818 E., González-Casado, J.M., Dahlquist, J.A., 2008. The Maz terrane: a Mesoproterozoic

819 domain in the western Sierras Pampeanas (Argentina) equivalent to the Arequipa-Antofalla

1 820 block of southern Peru? Implications for Western Gondwana margin evolution. *Gondwana*  
2 821 *Res.*, 13, 163-175.  
3  
4 822 Chew, D.M., Schaltegger, U., Kosler, J., Whitehouse, M.J., Gutjahr, M., Spikings, R.A.,  
5  
6 823 Miskovic, A., 2007. U-Pb geochronologic evidence for the evolution of the Gondwanan  
7  
8 824 margin of the north-central Andes. *Geological Society of America Bulletin*, 119, 697-711.  
9  
10 825 Cobbing, E.J., Pitcher, 1972. Plate tectonics and the Peruvian Andes. *Nature*, 246, 51-53.  
11  
12 826 Cobbing, E.J., Ozard, J.M., Snelling, N.J., 1977. Reconnaissance geochronology of the  
13  
14 827 crystalline basement of the Coastal Cordillera of southern Peru. *Geological Society of*  
15  
16 828 *America Bulletin*, 88, 241-246.  
17  
18 829 Copeland, P., Parrish, R.R., Harrison, T.M., 1988. Identification of inherited radiogenic Pb in  
19  
20 830 monazite and its implications for U-Pb systematics. *Nature*, 333, 760-763.  
21  
22 831 Cordani, U.G., Teixeira, W., 2007. Proterozoic accretionary belts in the Amazonian Craton.  
23  
24 832 In: Hatcher, R.D. Jr., Carlson, M.P. McBride, J.H., Martinez Catalán, J.R. (Eds.), 4-D  
25  
26 833 Framework of Continental Crust: *Geological Society of America, Memoir 200*, 297-320.  
27  
28 834 Cordani, U.G., Tassinari, C.C.G., Reis Rolim, D.R., 2005. The basement of the Rio Apa  
29  
30 835 Craton in Mato Grosso do Sul (Brazil) and northern Paraguay: a geochronological  
31  
32 836 correlation with tectonic provinces of the south-western Amazonian Craton. In: Pankhurst,  
33  
34 837 R.J. & Veiga, G.D. (Eds.), *Gondwana 12: Geological and Biological Heritage of*  
35  
36 838 *Gondwana. Abstracts, Academia Nacional de Ciencias, Córdoba, Argentina*, p.113.  
37  
38 839 Cordani, U.G., Tassinari, C.C.G., Teixeira, W., Coutinho, J.M.V., 2008. U-Pb SHRIMP  
39  
40 840 Zircon ages for the Rio Apa cratonic fragment in Mato Grosso do sul (Brazil) and northern  
41  
42 841 Paraguay: Tectonic implications. VI South American Symposium on Isotope Geology,  
43  
44 842 Bariloche, Argentina, Proceedings.  
45  
46  
47  
48  
49  
50  
51  
52  
53  
54  
55  
56  
57  
58  
59  
60  
61  
62  
63  
64  
65

- 843 Corfu, F., Hanchar, J.M., Hoskin, W.O., Kinny, P., 2003. Atlas of Zircon Textures. In:  
1  
2 844 Hanchar, J.M. and Hoskin, P.W.O. (Eds.), *Zircon, Reviews in Mineralogy and*  
3  
4 845 *Geochemistry*, 53, 469-500.
- 5  
6  
7 846 Dahlquist, J.A., Pankhurst, R.J., Rapela, C.W., Galindo, C., Alasino, P., Fanning, C.M.,  
8  
9 847 Saavedra, J., Baldo, E., 2008. New SHRIMP U-Pb data from the Famatina Complex:  
10  
11 848 constraining Early-Mid Ordovician Famatinian magmatism in the Sierras Pampeanas,  
12  
13 849 Argentina. *Geologica Acta*, 6, 319-333.
- 14  
15  
16  
17 850 Dalmayrac, B., Lancelot, J.R., Leyreloup, A., 1977. Two-billion year granulites in the Late  
18  
19 851 Precambrian metamorphic basement along the southern Peruvian coast. *Science*, 198, 49-  
20  
21 852 51.
- 22  
23  
24 853 Dalziel, I. W. D., 1997. Overview. Neoproterozoic-Paleozoic geography and tectonics: Review,  
25  
26 854 hypothesis, environmental speculation: *Geological Society of America Bulletin*, 109, p. 16-  
27  
28 855 42.
- 29  
30  
31 856 Davidson, A., 1995. A review of the Grenville orogen in its North American type area. *Journal*  
32  
33 857 *of Australian Geology and Geophysics*, 16, 3-24.
- 34  
35  
36 858 DePaolo, D.J., 1981. Neodymium isotopes in the Colorado Front Range and crust-mantle  
37  
38 859 evolution in the Proterozoic. *Nature*, 291, 193-196.
- 39  
40  
41 860 DePaolo, D.J., Linn, A.M., Schubert, G., 1991. The continental crustal age distribution:  
42  
43 861 methods of determining mantle separation ages from Sm-Nd isotopic data and application  
44  
45 862 to the Southwestern United States. *J. Geophys. Res.*, B96, 2071-2088.
- 46  
47  
48 863 Goodge, J.W., Vervoort, J.D., 2006. Origin of Mesoproterozoic A-type granites in Laurentia:  
49  
50 864 Hf isotope evidence. *Earth and Planetary Science Letters*, 243, 711-731.
- 51  
52  
53 865 Goodge, J.W., Fanning, M., Bennett, V.C., 2001. U-Pb evidence of ~ 1.7 Ga crustal tectonism  
54  
55 866 during the Nimrod Orogeny in the Transantarctic Mountains, Antarctica: implications for  
56  
57 867 Proterozoic plate reconstructions. *Precambrian Research*, 112, 261-288.
- 58  
59  
60  
61  
62  
63  
64  
65

- 1 868 Goodge, J.W., Williams, I.S., Myrow, P., 2004. Provenance of Neoproterozoic and lower  
2 869 Paleozoic siliciclastic rocks of the Central Ross orogen, Antarctica: detrital record of rift-,  
3  
4 870 passive-, and active-margin sedimentation. *Geological Society of America Bulletin*, 116,  
5  
6  
7 871 1253-1279.
- 8  
9 872 Hoffman, P.F., 1991. Did the breakout of Laurentia turn Gondwanaland inside out? *Science*,  
10  
11  
12 873 252, 1409-1412.
- 13  
14 874 Li, Z.X., et al., 2008, Assembly, configuration, and break-up history of Rodinia: A synthesis.  
15  
16 875 *Precambrian Research*, 160, 179-210.
- 17  
18  
19 876 Litherland, M., Annells, R.N., Darbyshire, D.P.F., Fletcher, C.J.N., Hawkins, M.P., Klinck, B.A.,  
20  
21 877 Mitchell, W.I., O'Connor, E.A., Pitfield, P.E.J., Power, G., Webb, B.C., 1989. The  
22  
23 878 Proterozoic of eastern Bolivia and its relationships to the Andean mobile belt. *Precambrian*  
24  
25 879 *Research*, 43, 157-174.
- 26  
27  
28 880 Loewy, S.L., Connelly, J.N., Dalziel, I.W.D. & Gower, C.F., 2003. Eastern Laurentia in Rodinia:  
29  
30 881 constraints from whole-rock Pb and U/Pb geochronology. *Tectonophysics*, 375, 169-197.
- 31  
32  
33 882 Loewy, S.L., Connelly, J.N. & Dalziel, I.W.D., 2004: An orphaned block: the Arequipa-  
34  
35 883 Antofalla basement of the central Andean margin of South America. *GSA Bulletin*, 116, 171-  
36  
37 884 187.
- 38  
39  
40 885 Ludwig, K.R., 2001. SQUID 1.02. A user's manual. Berkeley Geochronological Center  
41  
42 886 Special Publication, 2, 2455 Ridge Road, Berkeley, Ca 94709, USA.
- 43  
44  
45 887 Martignole, J., Martelat, J.E., 2003. Regional-scale Grenvillian-age UHT metamorphism in  
46  
47 888 the Mollendo-Camana Block (basement of the Peruvian Andes). *Journal of Metamorphic*  
48  
49 889 *Geology*, 21 (1), 99-120.
- 50  
51  
52 890 Martignole, J., Stevenson, R., Martelat, J.E., 2005. A Grenvillian anorthosite-mangerite-  
53  
54 891 charnockite-granite suite in the basement of the Andes: the Ilo AMCG site (southern Peru).  
55  
56 892 *IDSAG*, Barcelona, Extended Abstracts, 481-484.
- 57  
58  
59  
60  
61  
62  
63  
64  
65

- 893 Moores, E.M., 1991. Southwest U.S.-East Antarctic (SWEAT) connection: A Hypothesis.  
1  
2 894 Geology, 19, 425-428.  
3
- 4 895 Pankhurst, R.J., Rapela, C.W., Fanning, C.M., 2000. Age and origin of coeval TTTG, I- and  
5  
6 896 S-type granites in the Famatinian belt of NW Argentina. Transactions of the Royal Society  
7  
8 897 of Edimburgh: Earth Sciences 91, 151-168.  
9  
10
- 11 898 Parrish, R.R., 1990. U-Pb dating of monazite and its application to geological problems.  
12  
13 899 Canadian Journal Earth Sciences, 270, 1431-1450.  
14  
15
- 16 900 Priem, H.N.A., Boelrijk, N.A.I.M., Hebeda, E.H., Verdumen, E.A.T., Verschure, R.H. and  
17  
18 901 Bon, E.H., 1971. Granitic complexes and associated tin mineralization of Grenville age in  
19  
20 902 Rondonia, western Brasil. Geological Society of America Bulletin, 82, 4, 1095-1102.  
21  
22
- 23 903 Ramos, V.A., 1988. Late Proterozoic – Early Paleozoic of South America – a collisional  
24  
25 904 history. Episodes, 11, 168-174.  
26  
27
- 28 905 Restrepo-Pace P.A., Ruiz, J., Gehlers, G., Cosca, M., 1997. Geochronology and Nd isotopic  
29  
30 906 data of Grenville-age rocks in the Colombian Andes: new constraints fro Late Proterozoic  
31  
32 907 – Early Paleozoic paleocontinental reconstructions of the Amercias. Earth and Planetary  
33  
34 908 Science Letters, 150, 427-441.  
35  
36
- 37 909 Rivers, T., 1997, Lithotectonic elements of the Grenville Province: review and tectonic  
38  
39 910 implications. Precambrian Research, 86, 117-154.  
40  
41
- 42 911 Rivers, 2008. Assembly and preservation of lower, mid and upper orogenic crust in the  
43  
44 912 Grenville Province – Implications for the evolution of large hot long-duration orogens.  
45  
46 913 Precambrian Research, 167, 237-259.  
47  
48
- 49 914 Santos, J.O.S., Rizzotto, G.J., Potter, P.E., McNaughton, N.J., Matos, R.S., Hartmann, L.A.,  
50  
51 915 Chemale, F. Jr., Quadros, M.E.S., 2008. Age and autochthonous evolution of the Sunsás  
52  
53 916 Orogen in West Amazon Craton based on mapping and U-Pb geocronology. Precambrian  
54  
55 917 Research, 165, 120-152.  
56  
57  
58  
59  
60  
61  
62  
63  
64  
65

- 1  
2  
3  
4  
5  
6  
7  
8  
9  
10  
11  
12  
13  
14  
15  
16  
17  
18  
19  
20  
21  
22  
23  
24  
25  
26  
27  
28  
29  
30  
31  
32  
33  
34  
35  
36  
37  
38  
39  
40  
41  
42  
43  
44  
45  
46  
47  
48  
49  
50  
51  
52  
53  
54  
55  
56  
57  
58  
59  
60  
61  
62  
63  
64  
65
- 918 Shackleton, R.M., Ries, A.C., Coward, M.P., Cobbold, P.R. 1979. Structure, metamorphism  
919 and geochronology of the Arequipa massif of coastal Peru. *Journal of the Geological*  
920 *Society*, London, 136, 195-214.
- 921 Schulz, K.L., Cannon, W.F., 2007. The Penokean orogeny in the Lake Superior region.  
922 *Precambrian Research*, 157, 4-25.
- 923 Siivola, J., Schmid, R., 2007. List of Mineral Abbreviation. In: Fettes, D., Desmonds, J.  
924 (Eds.). *Metamorphic Rocks. A Classification and Glossary of Terms*. Cambridge  
925 University Press, p. 93-110.
- 926 Taylor, S.R., McLennan, S.M., 1988. The significance of the Rare Earths in geochemistry and  
927 cosmochemistry. In: Gschneider, K.A. Jr. and Eyring, L. (Eds.), *Handbook on the Physics*  
928 *and Chemistry of Rare Earths*, Elsevier Publ. B.V., 11, 486-578.
- 929 Tohver, E., Bettencourt, J.S., Tosdal, R., Mezger, K., Leite, W.B. and Payolla, B.L., 2004.  
930 Terrane transfer during Grenville orogeny: tracing the Amazonian ancestry of southern  
931 Appalachian basement through Pb and Nd isotopes. *Earth and Planetary Science Letters*,  
932 228, 161-176.
- 933 Tosdal, R.M., 1996. The Amazon-Laurentian connection as viewed from the Middle  
934 Proterozoic rocks in the Central Andes, western Peru and Northern Chile. *Tectonics*, 15,  
935 827-842.
- 936 Vavra, G., Schmid, R., Gebauer, D., 1999. Internal morphology, habit and U-Th-Pb  
937 microanalysis of amphibolite-to-granulite facies zircons: geochronology and the Ivrea  
938 Zone (Southern alps). *Contributions to Mineralogy and Petrology*, 134, 380-404.
- 939 Wasteneys, H.A., Clark, A.H., Farrar, E., Langridge, R.J., 1995. Grenvillian granulite-facies  
940 metamorphism in the Arequipa Massif, Peru: a Laurentia-Gondwana link. *Earth and*  
941 *Planetary Science Letters*, 132, 63-73.

1  
2 942 Whitmayer, S.J., Karlstrom, K.E., 2007. Tectonic model for the Proterozoic growth of North  
3 943 America. *Geosphere*, 3, 220-259.

4  
5 944 Williams, I.S., 1998. U-Th-Pb geochronology by ion microprobe. In: McKibben, M.A.,  
6  
7 945 Shanks, W.C. III, Ridley, W.I. (Eds.), *Applications of microanalytical techniques to*  
8  
9 946 *understanding mineralizing processes*. *Rev. Econ. Geol.*, 7, 1-35.

10  
11 947

12  
13 948

14  
15 949

16  
17 950

18  
19 951

20  
21 952

22  
23  
24 **953 Figures**

25  
26 954

27  
28  
29 955 Fig. 1 Sketch map of the Arequipa Massif showing domains distinguished in the text and  
30  
31 956 location of samples. Insets show the location of the Arequipa Massif in South America and  
32  
33 957 relationships with other pre-Andean outcrops in northern Chile and Argentina.

34  
35 958

36  
37 959 Fig. 2. a) Banded migmatitic gneisses near Quilca traversed by Cainozoic basaltic dykes. b)  
38  
39 960 Basement outcrop near Ilo. Mylonitic porphyritic granites (P) with disrupted anorthosite lenses  
40  
41 961 (A), and dark bands of fine-grained mylonitic gneisses (M).

42  
43 962

44  
45  
46 963 Fig. 3. U-Pb SHRIMP data for samples from the northern section of the Arequipa Massif.  
47  
48 964 <sup>204</sup>Pb-corrected data are plotted as 1σ error ellipses in Wetherill Concordia diagrams, with  
49  
50 965 typical cathodo-luminescence images displayed below. (a) MAR-8 (San Juan Marcona)  
51  
52 966 shows data for cores (grey shading) trending away from *ca.* 1800 Ma, interpreted as an

53  
54  
55  
56  
57  
58  
59  
60  
61  
62  
63  
64  
65

1 967 igneous protolith age, and rims (white ellipses) plotting on a Discordia between *ca.* 1000 Ma  
2 968 (Grenvillian age of main metamorphism) towards *ca.* 470 Ma (Famatinian overprint). (b)  
3  
4 969 OCO-26 (Atico) shows a rather discordant spread of data from Archaean to Neoproterozoic,  
5  
6  
7 970 with the  $^{207}\text{Pb}/^{206}\text{Pb}$  ages concentrating at *ca.* 1000 Ma (metamorphism).  
8

9 971  
10  
11 Fig. 4. U–Pb SHRIMP data for samples from the southern section of the Arequipa Massif.  
12 972  
13  
14 973  $^{204}\text{Pb}$ -corrected data are plotted as  $1\sigma$  error ellipses in Wetherill Concordia diagrams, with  
15  
16  
17 974 typical cathodo-luminescence images displayed below. (a) CAM-2 shows a strong bipolar  
18  
19 975 distribution of ages ( $^{206}\text{Pb}/^{238}\text{U}$  for  $<1000$  Ma,  $^{207}\text{Pb}/^{206}\text{Pb}$  for  $>1000$  Ma), indicating Pb-loss  
20  
21  
22 976 from a major events at *ca.* 1900 Ma and a second concentration around 1000 Ma. (b) CAM-7  
23  
24 977 and (c) QUI-16 show similar patterns with additional discordance (white ellipses indicate data  
25  
26  
27 978 ignored in the discordia fit). (d) MOL-17 from the Mollendo area (cathodo-luminescence  
28  
29 979 image shown below) also has three highly concordant data points for zircon rims at 940 Ma.  
30

31 980  
32  
33  
34 981 Fig. 5. U–Pb SHRIMP data for samples from the Ilo domain. Uncorrected data are plotted as  
35  
36  
37 982  $1\sigma$  error ellipses in Tera-Wasserburg diagrams. All data plot with Ordovician extrapolated  
38  
39 983 ages, but with a significant spread along Concordia. For (a) ILO-19 and (b) ILO-20, the insets  
40  
41 984 show attempts at unmixing the ages. For (c) ILO-23 (anorthosite) insufficient data were  
42  
43  
44 985 obtainable for detailed treatment, but the cathodo-luminescence image inset shows good  
45  
46  
47 986 igneous concentric zoning to support interpretation of the magmatic crystallization as  
48  
49 987 Ordovician in age.  
50

51 988  
52  
53  
54 989 Fig. 6. Chondrite-normalized REE patterns of migmatitic gneisses. The North America Shale  
55  
56 990 Composite REE pattern (Taylor and McLennan, 1988) is added for comparison.  
57

58 991  
59  
60  
61  
62  
63  
64  
65



992 Fig. 7. Paleogeographical reconstruction of Laurentia and Amazonia at *ca.* 1.2 Ga (Tohver et  
1  
2 993 al., 2004), showing Precambrian orogenic belts with ages according to Goodge et al. (2004,  
3  
4 994 fig. 16), Tohver et al. (2004) and Cordani and Teixeira (2007). Outcrops of basement with  
5  
6  
7 995 Grenvillian ages in southern Laurentia and in the Central Andean region (Peru, NW Chile and  
8  
9  
10 996 Argentina) have been included (the latter in its present position relative to Amazonia).  
11  
12 997 Laurentia: TH, Trans Hudson and related mobile belts; P, Penokean orogen; Y, Yavapay  
13  
14 998 orogen; M, Mazatzal orogen; GR, Granite-Rhyolite province; FM, Franklin mountains  
15  
16  
17 999 outcrop; VHM, Van Horn Mountains outcrop; LU, Llano Uplift outcrop. Amazonía: MI,  
18  
19 1000 Maroni–Itacaiunas Province; CA, Central Amazonia province; VT, Venturi-Tapajós province;  
20  
21  
22 1001 RNJ, Rio Negro Jurena province; R, Rondonia–San Ignacio province; Sunsás, orogenic belts  
23  
24 1002 of Grenvillian age along southern Amazonía; AM, Arequipa Massif (Peru); RA, Rio Apa  
25  
26  
27 1003 outcrop (Brasil, Paraguay); WSP, Western Sierras Pampeanas (Argentina); G, Garzón massif  
28  
29 1004 (Colombia); ST, Santander massif (Colombia).  
30  
31 1005  
32  
33  
34  
35  
36  
37  
38  
39  
40  
41  
42  
43  
44  
45  
46  
47  
48  
49  
50  
51  
52  
53  
54  
55  
56  
57  
58  
59  
60  
61  
62  
63  
64  
65

Figure1

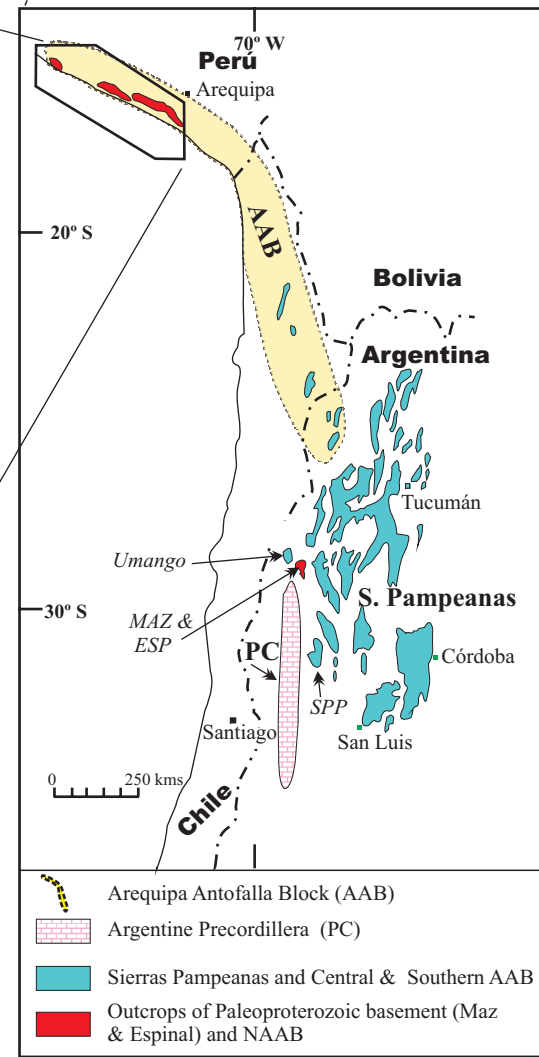
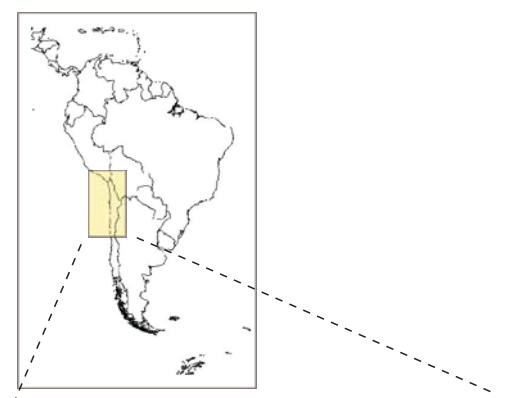
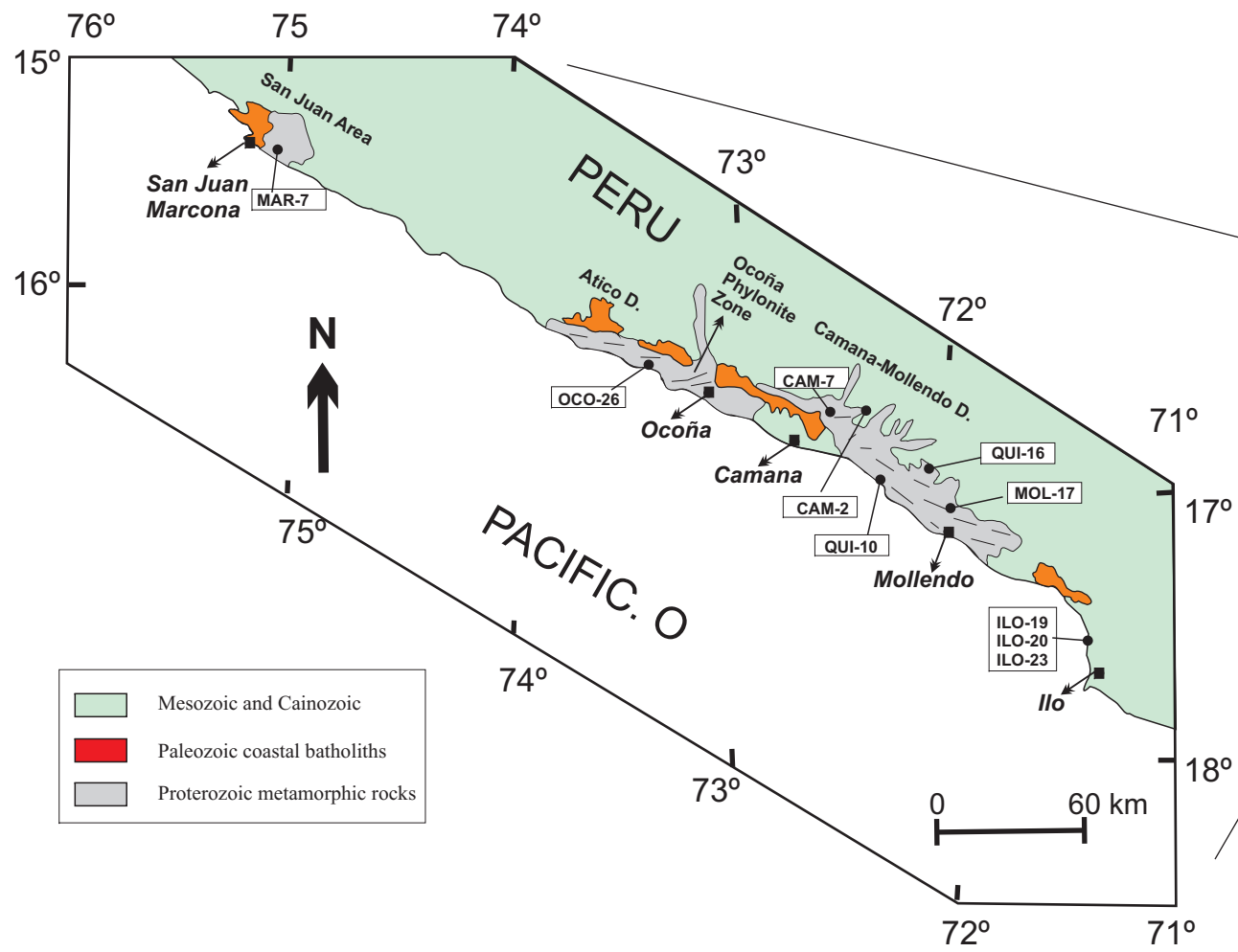


Fig. 1

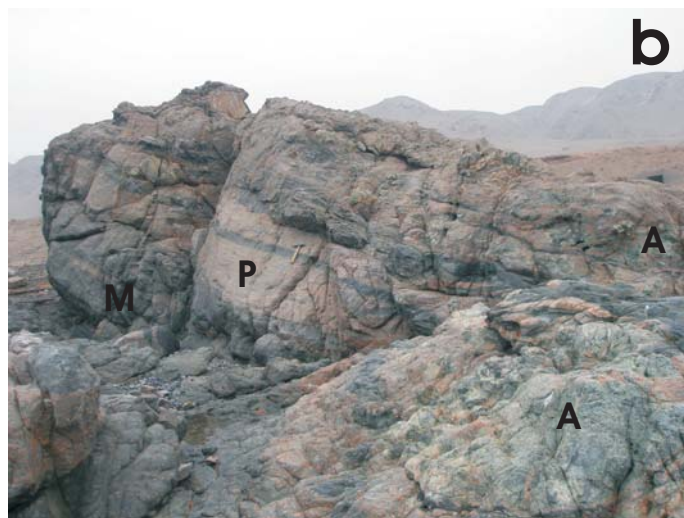
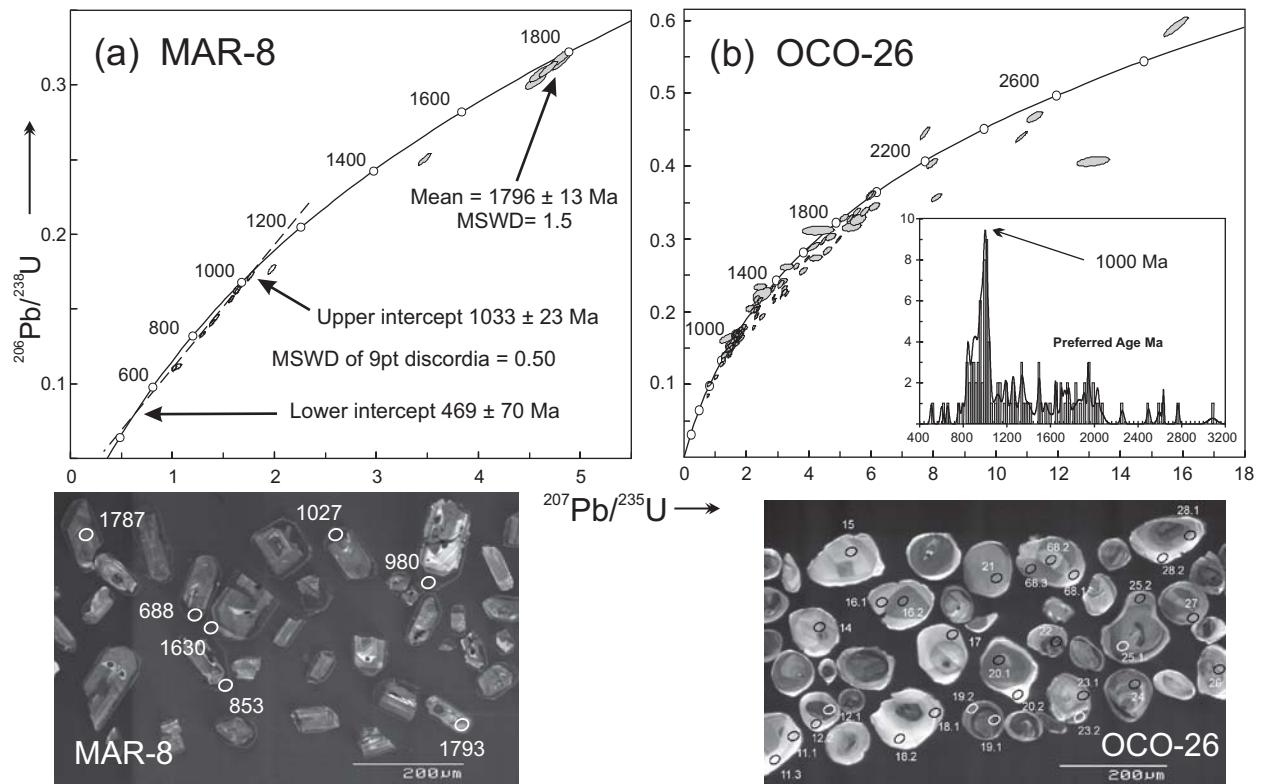


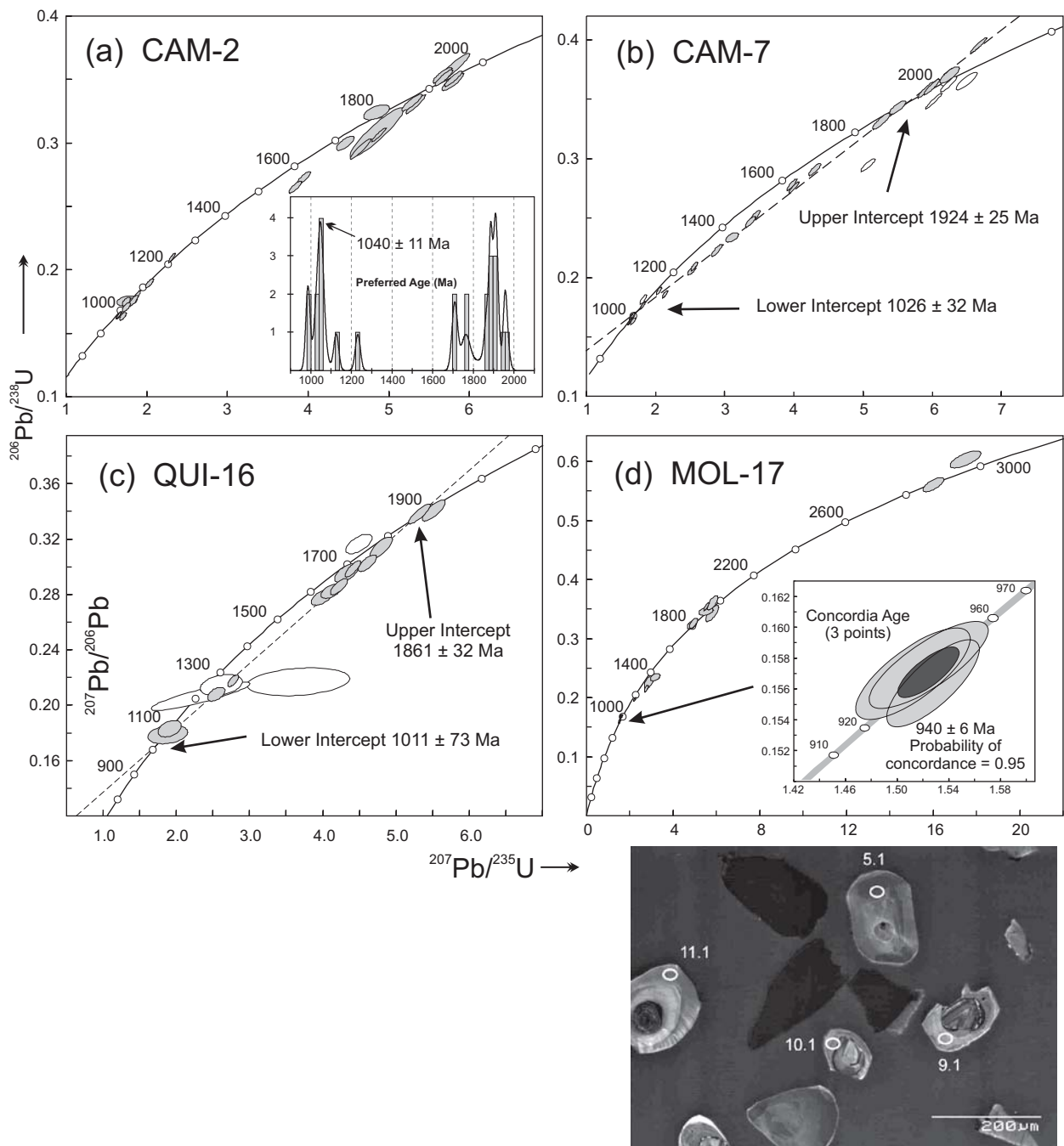
Fig. 2

Figure 3



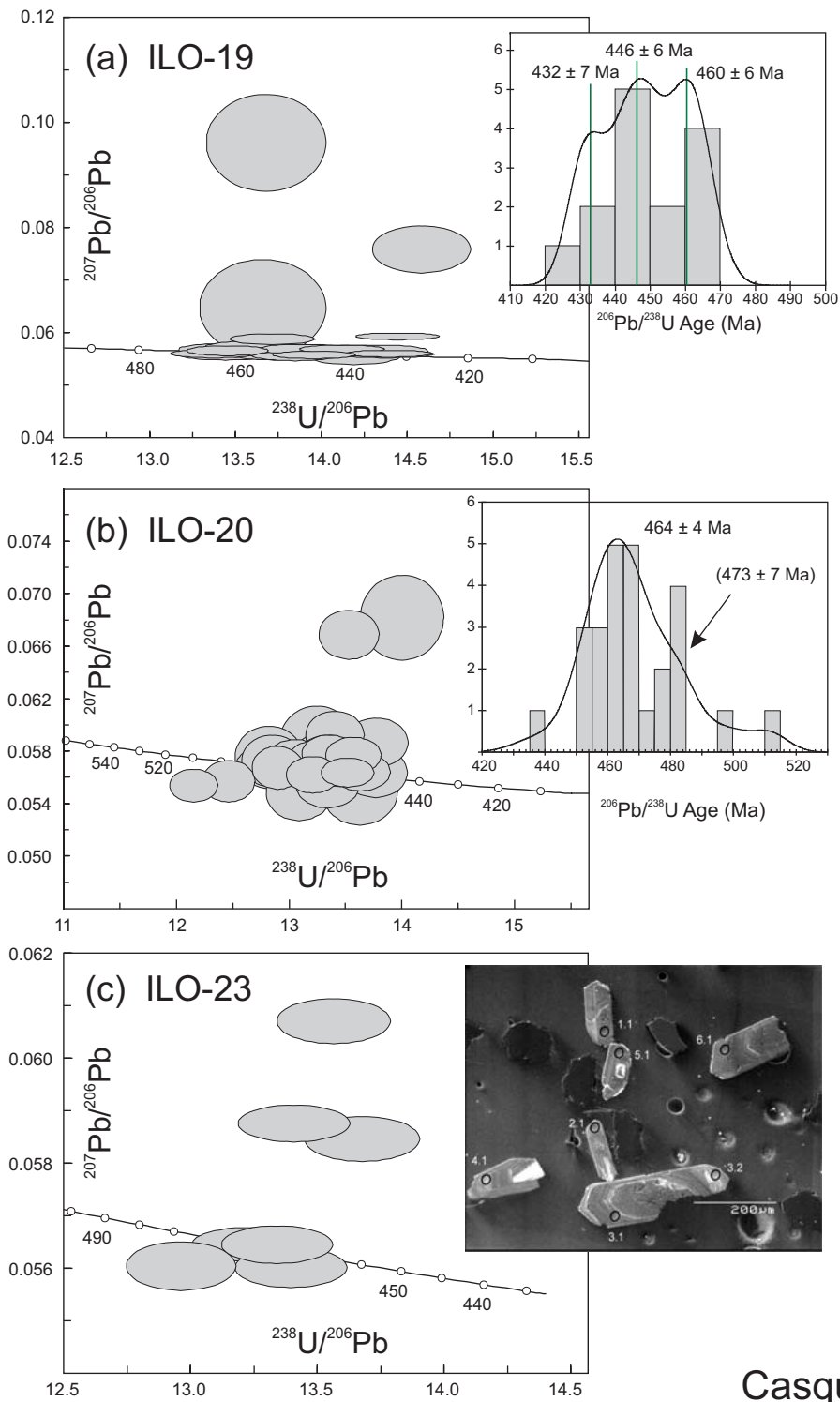
Casquet et al. Fig 3

Figure 4



Casquet et al. Fig 4

Figure5



Casquet et al. Fig 5  
(one column)

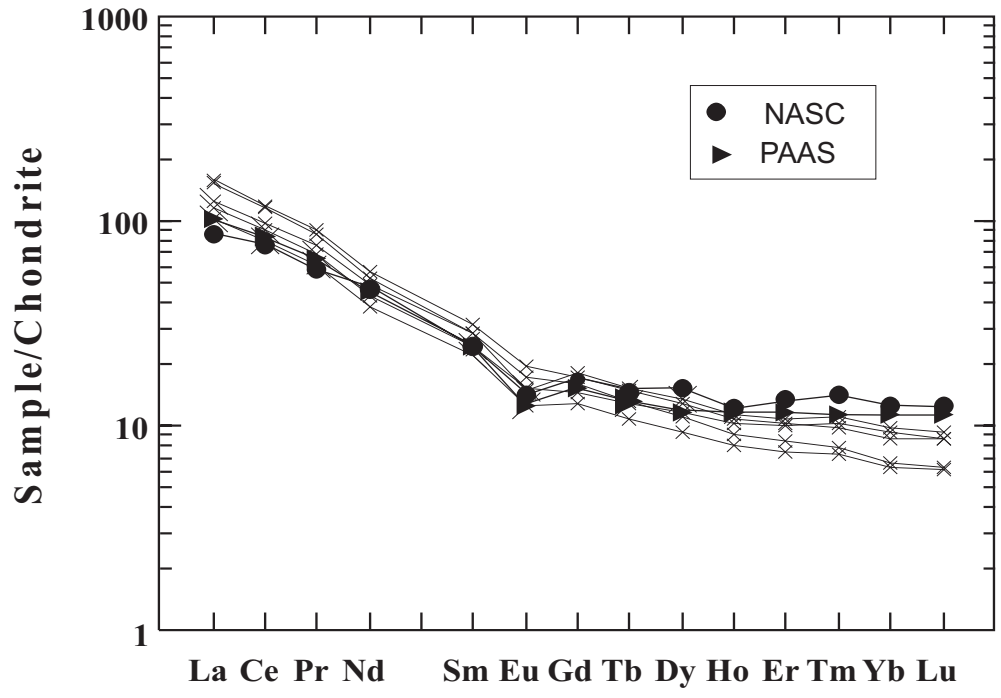


Fig.6

Figure7

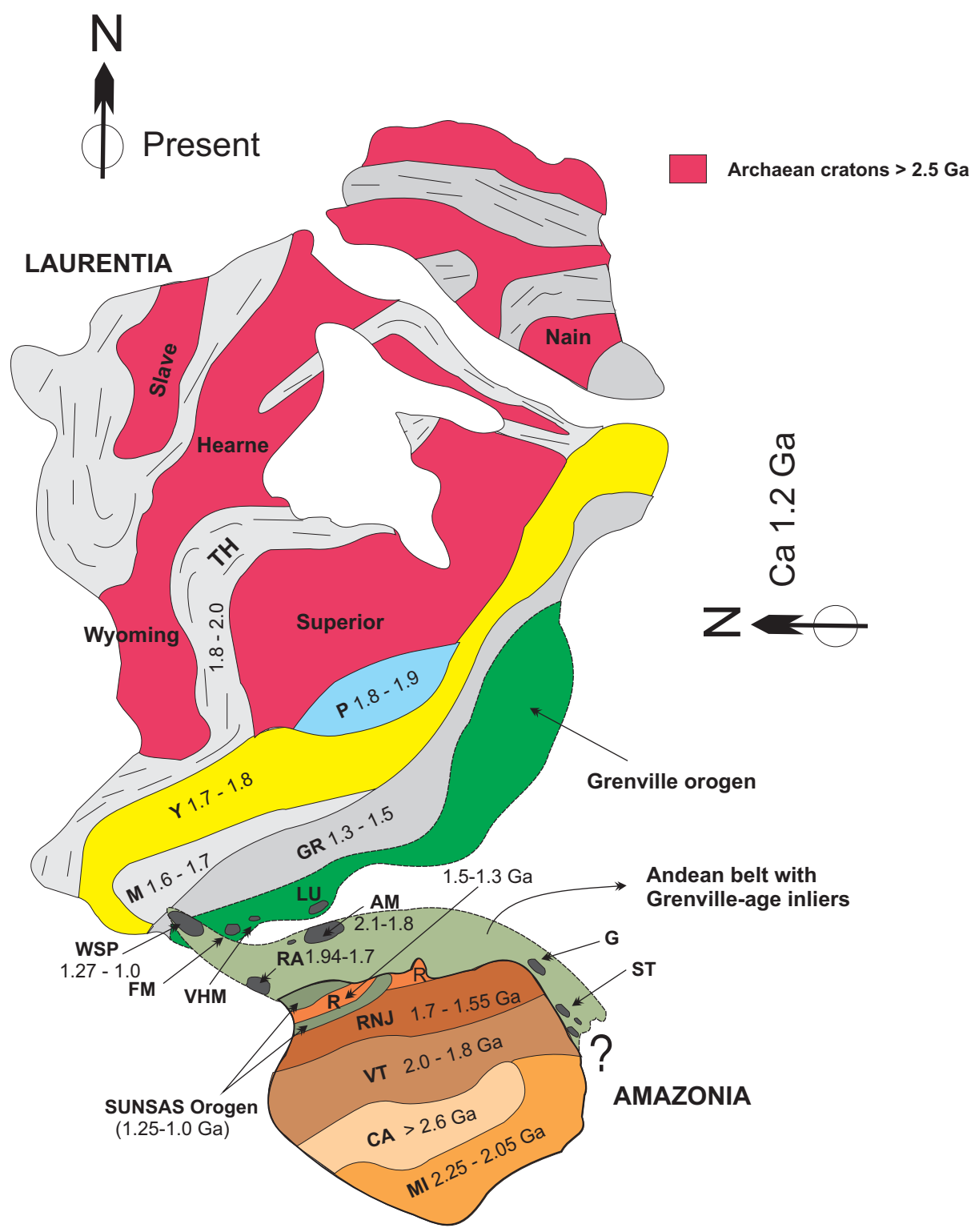


Fig. 7



Table 1

1  
2  
3  
4  
5  
67 **TABLE 1. Short description of rocks selected for U-Pb SHRIMP zircon dating and geochemistry**

8	Sample	coordinates	domain	rock type*	abbreviated mineralogy**	Anal. work
10	MAR-8	15°24'21.3''S, 75°08'16.8''W	S. Juan Marcona	Fine-grained gneiss. Dacitic to rhyodacitic. Low-grade retrogression: strong	Qtz, Pl, Kfs, Ms, Chl, Op, Cb, Zrn	S
11	OCO-26	16°26'32.5''S, 73°07'24.7''W	S. Juan Marcona	Medium-grade metasandstone	Qtz, Pl, Ms, Bt, Zrn	S
12	CAM-2	16°32'17.2''S, 72°31'23.2''W	Camaná-Mollendo	Banded migmatitic gneiss	Qtz, Pl, Kfs, Opx, Sil, Bt, Mag, Zrn	S, I, R
13	CAM-6	16°30'40.3''S, 72°38'16.6''W	""	Gneiss (mesosome)	Qtz, Kfs, Pl, Grt, Sill, Mag, Bt, Chl, Ser, Zr, Ap, Sp	I, R
14	CAM-7	16°30'40.3''S, 72°38'16.6''W	Camaná-Mollendo	Banded migmatitic gneiss	Qtz, Kfs, Pl, Grt, Sil, Bt, Mag, Zrn	S, I, R
15	QUI-10	16°42'52.9''S, 72°25'18.9''W	""	Banded migmatitic gneiss	Qtz, Kfs, Sill, Bt, Opx, Pl, Mag, Chl, Ser, Zrn, Ap	I, R
16	QUI-16	16°40'59.3''S, 72°20'05.9''W	""	Banded migmatitic gneiss	Qtz, Pl, Kfs, Bt, Sill, Grt, Mag, Ser, Chl, Zrn	S, I, R
17	MOL-17	16°54'59.2''S, 72°02'50.4''W	Camaná-Mollendo	Augen-gneiss	Qtz, Kfs, Pl, Grt, Sil, Mag, Bt, Ser, Ep, Chl, Zrn	S
18	ILO-19	17°27'59.2''S, 71°22'19.9''W	Ilo	Reddish mylonitic porphyritic granite. Low-grade retrogression: strong	Qtz, Chl, Ep, Pl, Kfs, Ttn, Ilm, Ser, Aln, Ap, Fl, Zr	S, I, R
19	ILO-20	17°27'59.2''S, 71°22'19.9''W	Ilo	Mylonitic dark gneiss. Low grade retrogression: moderate	Qtz, Pl, Hb, Bt, Chl, Ser, Ep, Aln, Mt, Ap, Zrn	S, I, R
20	ILO-23	17°28'56.1''S, 71°21'56.4''W	Ilo	Coarse grained anorthosite. Low grade retrogression: minor	Pl, Hb, Bt, Ttn, Rt, Ilm, Ser, Chl, Ep	S, I, R

27 \* For a detailed description see supplementary table in Data Repository

28 \*\*Mineral abbreviations according to Siivola and Schmid (2007). Order reflects relative modal amounts.

29 Analytical work: S = U-Pb SHRIMP; I = Nd isotope composition; R = REEs chemical analysis

30  
31  
32  
33  
34  
35  
36  
37  
38  
39  
40  
41  
42  
43  
44  
45  
46  
47  
48  
49

Table 2. Sm-Nd isotope composition of selected rocks from the Camana-Mollendo and Ilo domains.

Sample	Sm ppm	Nd ppm	Sm/Nd	$^{147}\text{Sm}/^{144}\text{Nd}$	$^{143}\text{Nd}/^{144}\text{Nd}$	eNd <sub>465</sub>	T <sub>DM</sub> <sup>*</sup> (465)	eNd <sub>1000</sub>	eNd <sub>1700</sub>	T <sub>DM</sub>
CAM-2	5.59	30.3	0.1845	0.1115	0.511333			-14.6	-6.9	2445
CAM-6	6.57	34.4	0.1910	0.1154	0.511348			-14.8	-7.5	2513
CAM-7	5.1	27.1	0.1882	0.1137	0.511294			-15.6	-8.2	2549
QUI-10	7.3	39.9	0.1830	0.1106	0.511322			-14.7	-6.9	2440
QUI-16	6.57	37.5	0.1752	0.1059	0.511343			-13.7	-5.5	2314
ILO-19	8.01	50.7	0.1580	0.0955	0.511996	-6.4	1691			
ILO-20	10	60	0.1667	0.1007	0.511940	-7.8	1791			
ILO-23	1.02	4.46	0.2287	0.1383	0.512274	-3.6	1483			

Nd isotopic ratios were normalized to  $^{146}\text{Nd}/^{144}\text{Nd} = 0.7219$ .

La Jolla Nd standard gave a mean  $^{143}\text{Nd}/^{144}\text{Nd}$  of  $0.511847 \pm 0.00001$  (n = 9).

The  $2\sigma$  analytical errors are 0.1% in  $^{147}\text{Sm}/^{144}\text{Nd}$  and 0.006% in  $^{143}\text{Nd}/^{144}\text{Nd}$ .

Decay constant was  $\lambda_{\text{Sm}} = 6.54 \times 10^{-12} \text{ a}^{-1}$ .

T<sub>DM</sub><sup>\*</sup> is model age according to DePaolo *et al.* (1991).

$^{147}\text{Sm}/^{144}\text{Nd}$  and  $^{143}\text{Nd}/^{144}\text{Nd}$  values assumed to be 0.1967 and 0.512636 for CHUR, and 0.222 and 0.513114 for depleted mantle respectively

**Table 3. Rb-Sr composition of muscovite from pegmatites**

Sample	Rb	Sr	Rb/Sr	<sup>87</sup> Rb/ <sup>86</sup> Sr	<sup>87</sup> Sr/ <sup>86</sup> Sr	model age Ma
JC-01C Ms	609.412	6.52	93.4681	463.637	8.011008	1100
QUI-005 Ms	526.469	6.664	79.0020	338.286	5.614221	1015

Sr isotopic ratios were normalized to  $^{86}\text{Sr}/^{88}\text{Sr} = 0.1194$ .

NBS987 standard gave a mean  $^{87}\text{Sr}/^{86}\text{Sr}$  ratio of  $0.710216 \pm 0.00005$  (n = 10).

The  $2\sigma$  analytical errors are 1% in  $^{87}\text{Rb}/^{86}\text{Sr}$ , 0.01% in  $^{87}\text{Sr}/^{86}\text{Sr}$ .

Decay constants used were  $\lambda_{\text{Rb}} = 1.42 \times 10^{-11} \text{ a}^{-1}$ .

Model ages assumes initial  $^{87}\text{Sr}/^{86}\text{Sr}$  values between 0.703 and 0.715

Table 4. REE analyses of granulites

	CAM-2	CAM-6	CAM-7	QUI-10	QUI-16
La	42.8	46.4	37.7	58.1	55.3
Ce	86.1	93.2	76.8	115	110
Pr	9.46	10.5	8.43	12.4	11.8
Nd	30.3	34.4	27.1	39.9	37.5
Sm	5.59	6.57	5.1	7.3	6.57
Eu	1.32	1.28	1.1	1.71	1.5
Gd	4.44	5.54	3.94	5.32	4.88
Tb	0.75	0.89	0.63	0.86	0.76
Dy	4.44	5.09	3.56	4.93	4.21
Ho	0.88	0.96	0.68	0.92	0.77
Er	2.49	2.72	1.84	2.55	2.1
Tm	0.364	0.393	0.257	0.345	0.277
Yb	2.28	2.42	1.57	2.15	1.62
Lu	0.333	0.351	0.235	0.326	0.241
REE	191.5	210.7	168.9	251.8	237.5
(La/Yb)N	13.5	13.8	17.2	19.4	24.5
(La/Sm)N	4.9	4.6	4.8	5.1	5.4
(Gd/Yb)N	1.6	1.9	2.1	2.0	2.5
Eu/Eu*	0.8	0.6	0.8	0.8	0.8

e-component1

[Click here to download e-component: Supplementary data #1.pdf](#)

e-component2

[Click here to download e-component: Supplementary data # 2.pdf](#)